III. 研究成果の刊行に関する一覧

研究成果の刊行に関する一覧表
【H24. 4. 1～H25. 3. 31】

雑誌

発表者氏名	論文タイトル名	発表誌名	巻号	ページ	出版年
Asagiri M et al.	Control of RelB during dendritic cell activation integrates canonical and noncanonical NF-κB pathways.	Nature Immunol.	13(12)	1162-70.	2012
Asagiri M et al.	Epidermal phospholipase Cδ1 regulates granulocyte counts and systemic interleukin-17 levels in mice.	Nature Commun.	3	963	2012
Iwaisako K et al.	Protection from liver fibrosis by a peroxisome proliferator-activated receptor δ agonist.	Proc Natl Acad Sci U S A.	109(21)	E1369-76.	2012
Iwaisako K. et al.	What's new in liver fibrosis? The origin of myofibroblasts in liver fibrosis.	Journal of Gastroenterology and Hepatology	27	65-8	2012

IV. 研究成果の刊行物・別刷

nature immunology

Control of RelB during dendritic cell activation integrates canonical and noncanonical NF-κB pathways

Vincent F-S Shih[1], Jeremy Davis-Turak[1], Monica Macal[2], Jenny Q Huang[1], Julia Ponomarenko[3], Jeffrey D Kearns[1,5], Tony Yu[1], Riku Fagerlund[1], Masataka Asagiri[1,4], Elina I Zuniga[2] & Alexander Hoffmann[1]

The NF-κB protein RelB controls dendritic cell (DC) maturation and may be targeted therapeutically to manipulate T cell responses in disease. Here we report that RelB promoted DC activation not as the expected RelB-p52 effector of the noncanonical NF-κB pathway, but as a RelB-p50 dimer regulated by canonical IκBs, IκBα and IκBε. IκB control of RelB minimized spontaneous maturation but enabled rapid pathogen-responsive maturation. Computational modeling of the NF-κB signaling module identified control points of this unexpected cell type–specific regulation. Fibroblasts that we engineered accordingly showed DC-like RelB control. Canonical pathway control of RelB regulated pathogen-responsive gene expression programs. This work illustrates the potential utility of systems analyses in guiding the development of combination therapeutics for modulating DC-dependent T cell responses.

DCs are specialized sentinel immune cells essential in both innate and adaptive immunity. DC progenitors differentiate to become immature DCs that populate both nonlymphoid and lymphoid tissues and perform immune-surveillance functions. When encountering pathogens or pathogen-associated molecular patterns (PAMPs), immature DCs undergo a maturation program that determines their role in the adaptive immune response[1]. A hallmark of DC maturation is expression of major histocompatibility complex molecules (MHC), T cell co-stimulatory molecules (CD40, CD80 or CD86) and cytokines (for example, interleukin 23; IL-23) in addition to a gene expression program of intracellular factors that enable effective antigen uptake, processing and presentation, and T cell activation. In addition, production of inflammatory molecules such as nitric oxide and cytokines such as tumor necrosis factor (TNF) and interferon underlies DC functions in innate immune responses[2,3]. DCs have thus attracted attention for engineering or modulating immune-based therapies[4].

The transcription factor NF-κB protein RelB is highly expressed in antigen-presenting cells[5] and is critical for DC maturation, DC function as antigen-presenting cells[6] and DC-mediated immunity. Specifically, small interfering RNA–mediated silencing of RelB expression radically alters the DC maturation process and results in blunted antigen-specific T cell responses *in vitro* and *in vivo*[7]. RelB-deficient mice have deficiencies in splenic DC subsets[8,9] but other critical roles of RelB in DCs may be masked by other cell types in which RelB-deficiency leads to functionally opposite phenotype: notably, T cells are hyperactive in these null mice, whereas DC-specific deletion of the RelB-controlling kinase NIK results in deficient T cell responses[10]. Indeed, the extent of RelB activation determines the tolerance or rejection of allogenic organ transplants by determining the balance of associated activated or regulatory T cells[7]. These insights have prompted investigations of cell-based therapies for autoimmune diseases using RelB-silenced DCs[11].

Despite the potential clinical importance of RelB, the molecular mechanisms that control its activity in DCs have remained unclear. Mouse embryonic fibroblasts (MEFs) have served as a useful model system for many signaling studies. Detailed biochemical studies in MEFs have shown that unlike classical NF-κB (the RelA-p50 dimer), RelB is not activated from a latent cytoplasmic pool via the NEMO-dependent, 'canonical' signaling pathway but via the 'noncanonical' NF-κB pathway that involves proteolysis and processing of newly synthesized NF-κB2 p100[12–14]. Consistent with the critical role of RelB in DCs, noncanonical signaling pathway components such as the signaling protein NIK and *Nfkb2* gene have been reported to be required for proper DC functions[10,15]. However, RelB has also been found to be rapidly activated in DCs by canonical pathway stimuli TNF and lipopolysaccharide (LPS)[16–19], and the canonical signaling pathway component TRAF6 has been shown to be essential[9]. These reports suggest that the mechanism by which RelB activity is controlled in DCs may be different than what has been described in MEFs. In DCs, the molecular control mechanisms must provide for constitutive RelB expression to enable rapid and decisive induction of maturation programs after exposure to pathogens or PAMPs but must limit spontaneous maturation of DCs in their absence.

In this study, we elucidated the molecular mechanisms responsible for regulating RelB in DCs. We used a systems biology approach of iterative computational modeling and quantitative experimental

[1]Signaling Systems Laboratory, Department of Chemistry and Biochemistry and San Diego Center for Systems Biology, University of California, San Diego, La Jolla, California, USA. [2]Division of Biological Sciences, University of California, San Diego, La Jolla, California, USA. [3]San Diego Supercomputer Center, University of California, San Diego, La Jolla, California, USA. [4]Innovation Center for Immunoregulation and Therapeutics, Graduate School of Medicine, Kyoto University, Yoshida-Konoe, Sakyoku, Kyoto, Japan. [5]Present address: Merrimack Pharmaceuticals, Cambridge, Massachusetts, USA. Correspondence should be addressed to A.H. (ahoffmann@ucsd.edu).

Received 28 November 2011; accepted 29 August 2012; published online 21 October 2012; doi:10.1038/ni.2446

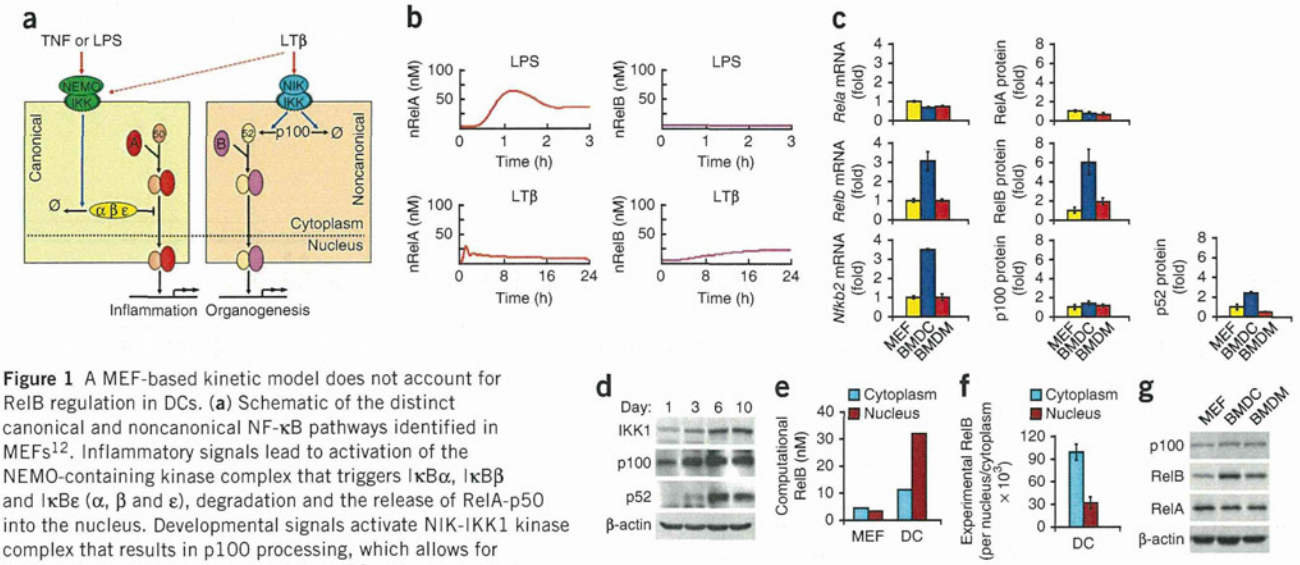

Figure 1 A MEF-based kinetic model does not account for RelB regulation in DCs. (**a**) Schematic of the distinct canonical and noncanonical NF-κB pathways identified in MEFs[12]. Inflammatory signals lead to activation of the NEMO-containing kinase complex that triggers IκBα, IκBβ and IκBε (α, β and ε), degradation and the release of RelA-p50 into the nucleus. Developmental signals activate NIK-IKK1 kinase complex that results in p100 processing, which allows for RelB-p52 nuclear translocation. (The IκBδ pathway is not shown for sake of clarity[21]). A, RelA; B, RelB; 50, p50; 52, p52; and Ø, sink (from which proteins are synthesized and into which they are degraded). (**b**) Computational simulations using the MEF-based kinetic model version 5.0–MEF (**Supplementary Note**) of nuclear RelA or RelB activity (nRelA and nRelB, respectively) induced by LPS or LTβ stimulation. (**c**) Quantification of *Rela*, *Relb* and *Nfkb2* transcripts by quantitative RT-PCR (left) and of RelA, RelB, p100 and p52 proteins by immunoblot (right); numbers per cell in resting MEFs, BMDMs and BMDCs, graphed relative to the respective value in MEFs. (**d**) IKK1 and p52 abundance increase during DC differentiation. Whole-cell extracts prepared from BMDC culture during a differentiation time course (days 1–10) were subjected to IKK1, p100 and p52 immunoblotting. β-actin served as a loading control. (**e**) *In silico* simulation of RelB cellular distribution using the mathematical model version 5.0–MEF describing NF-κB activation in MEFs as in **b** or in model version 5.0–DC incorporating DC-specific parameters derived from **c**,**d** (**Supplementary Note**). (**f**) Quantification of RelB molecules per wild-type (WT) BMDC distributed in cytoplasmic and nuclear fraction. Quantification methods are described in **Supplementary Figure 1**. (**g**) RelB, RelA and p100 immunoblots of cytoplasmic extracts prepared from the indicated cell types. Data are representative of at least three independent experiments (error bars, s.d.; $n = 3$).

analyses of the NF-κB signaling network in DCs to reveal that RelB activity was limited by classical IκBs, IκBα and IκBε, and regulated via the canonical pathway. Modeling studies identified two DC-specific control points that render RelB subject to regulation by the canonical pathway, and we demonstrated their sufficiency by engineering MEFs accordingly to produce DC-like RelB control. Finally, gene expression profiling revealed that RelB-dependent gene expression programs regulated by the canonical pathway activity control DC-orchestrated immune responses.

RESULTS

Developing a DC-specific model for NFκB signaling

The established view of NF-κB signaling comprises two separate pathways (**Fig. 1a**)[12]. The canonical pathway, involving the NEMO-dependent kinase IKK, triggers degradation of NF-κB inhibitors, the classical IκBs: IκBα, IκBβ and IκBε. Resulting activation of latent RelA-containing and c-Rel-containing NF-κB dimers controls inflammatory and proliferative gene expression programs. The noncanonical pathway, involving the kinases NIK and IKK1, triggers processing of p100 to p52 and generation of the RelB-p52 transcription factor, which is implicated in cell survival and maturation. To examine NF-κB RelB signaling in DCs in a quantitative manner, we developed a mathematical model that describes the formation and regulation of RelA and RelB dimers in terms of mass-action kinetics (**Supplementary Note**). The first version of the model involves 41 molecular species, 132 reactions and 53 unique kinetic parameters based on published and newly made measurements that constrain the model to a single parameter set ensemble; it recapitulates well-documented NF-κB control in MEFs[20–22], such as prompt LPS-induced RelA activation and delayed lymphotoxin β–mediated RelB activation (**Fig. 1b**).

To adapt the model to DCs, we first measured the expression of key NF-κB proteins in bone marrow–derived DCs (BMDCs) in comparison to that in MEFs and bone marrow–derived macrophages (BMDMs). Relative to the expression of the housekeeping gene β-actin (*Actb*), expression of *Rela* mRNA was similar in BMDCs, BMDMs and MEFs, and the relative amount of RelA protein in these cell types correlated (**Fig. 1c**). In contrast, we observed threefold to sixfold more *Relb* mRNA and protein expression in BMDCs than MEFs and BMDMs (**Fig. 1c** and **Supplementary Fig. 1a**). p100, encoded by the *Nfkb2* gene, is known to inhibit RelB. We therefore tested whether p100 expression correlated with enhanced RelB expression in BMDCs. We observed 3.5-fold more *Nfkb2* mRNA in BMDCs, but quantitative immunoblotting showed little difference in the p100 protein abundance among the cell types analyzed (**Fig. 1c** and **Supplementary Fig. 1b**). Lack of correlation between the relative p100 protein and RNA abundance suggested that p100 degradation may be elevated in BMDCs. We noted a 2.5-fold increase in the amount of p52 in BMDCs, which suggests that both complete p100 degradation and p100 processing to p52 may occur in BMDCs (**Fig. 1c** and **Supplementary Fig. 1b**). Consistent with this hypothesis, protein expression of IKK1, the kinase determining the activity of noncanonical NF-κB pathway, gradually increased during DC differentiation with concomitant p100 processing to p52 (**Fig. 1d**), potentially via the control of microRNAs[23]. Our data indicate that DC differentiation involves not only increased expression of RelB but also elevated constitutive activity of the noncanonical NF-κB signaling pathway.

Based on the measurements, we made specific modifications to the computational model to recapitulate RelB control in DCs (**Supplementary Note**). First, we increased *Relb* and *Nfkb2* expression threefold, which increased the abundance of RelB but not its

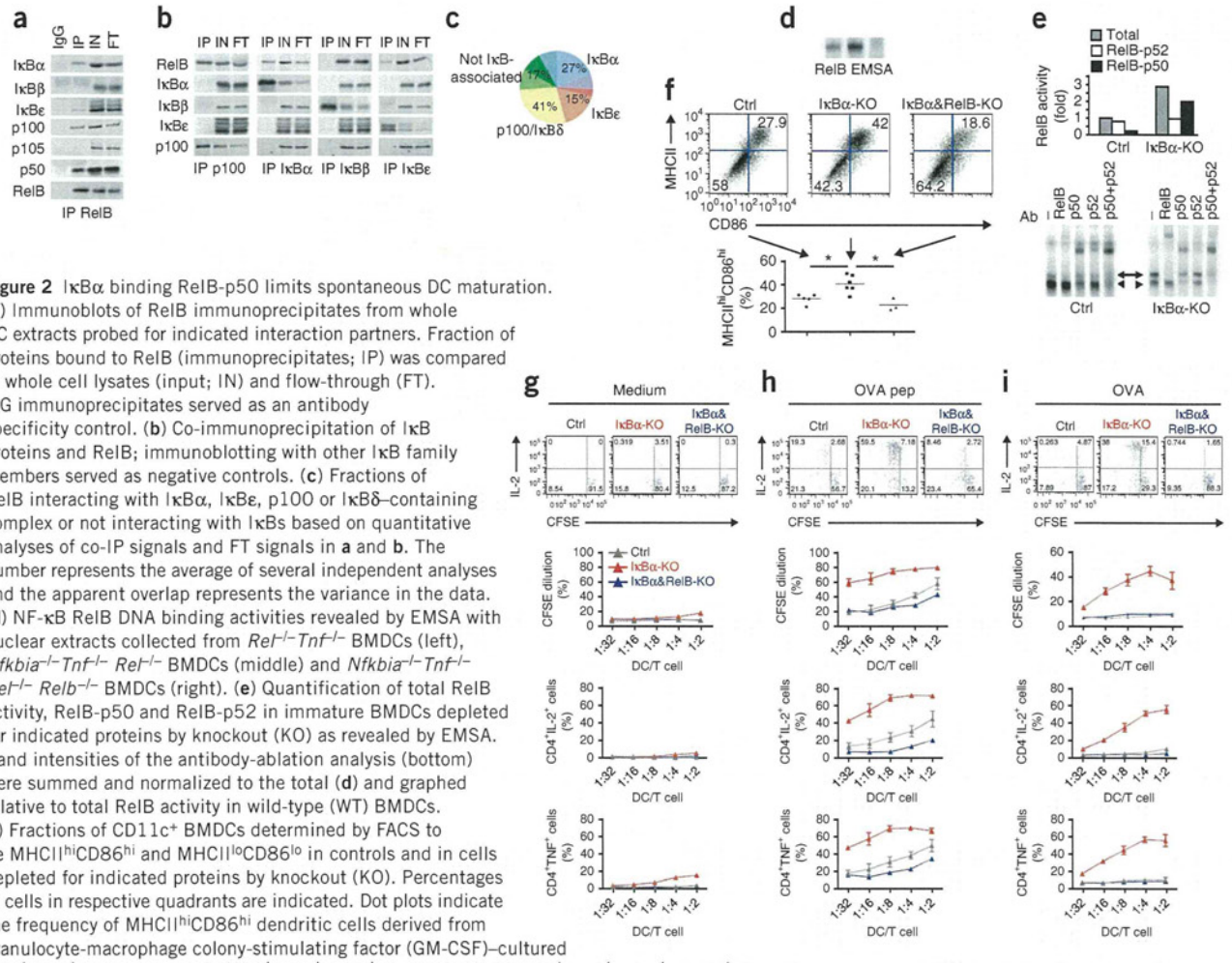

Figure 2 IκBα binding RelB-p50 limits spontaneous DC maturation. (**a**) Immunoblots of RelB immunoprecipitates from whole DC extracts probed for indicated interaction partners. Fraction of proteins bound to RelB (immunoprecipitates; IP) was compared to whole cell lysates (input; IN) and flow-through (FT). IgG immunoprecipitates served as an antibody specificity control. (**b**) Co-immunoprecipitation of IκB proteins and RelB; immunoblotting with other IκB family members served as negative controls. (**c**) Fractions of RelB interacting with IκBα, IκBε, p100 or IκBδ–containing complex or not interacting with IκBs based on quantitative analyses of co-IP signals and FT signals in **a** and **b**. The number represents the average of several independent analyses and the apparent overlap represents the variance in the data. (**d**) NF-κB RelB DNA binding activities revealed by EMSA with nuclear extracts collected from *Rel*$^{-/-}$*Tnf*$^{-/-}$ BMDCs (left), *Nfkbia*$^{-/-}$*Tnf*$^{-/-}$ *Rel*$^{-/-}$ BMDCs (middle) and *Nfkbia*$^{-/-}$*Tnf*$^{-/-}$ *Rel*$^{-/-}$ *Relb*$^{-/-}$ BMDCs (right). (**e**) Quantification of total RelB activity, RelB-p50 and RelB-p52 in immature BMDCs depleted for indicated proteins by knockout (KO) as revealed by EMSA. Band intensities of the antibody-ablation analysis (bottom) were summed and normalized to the total (**d**) and graphed relative to total RelB activity in wild-type (WT) BMDCs. (**f**) Fractions of CD11c$^+$ BMDCs determined by FACS to be MHCII^{hi}CD86^{hi} and MHCII^{lo}CD86^{lo} in controls and in cells depleted for indicated proteins by knockout (KO). Percentages of cells in respective quadrants are indicated. Dot plots indicate the frequency of MHCII^{hi}CD86^{hi} dendritic cells derived from granulocyte-macrophage colony-stimulating factor (GM-CSF)–cultured *Rel*$^{-/-}$*Tnf*$^{-/-}$ cells ($n = 5$), *Nfkbia*$^{-/-}$*Tnf*$^{-/-}$ *Rel*$^{-/-}$ ($n = 6$), and *Nfkbia*$^{-/-}$*Tnf*$^{-/-}$ *Rel*$^{-/-}$ *Relb*$^{-/-}$ ($n = 3$) bone marrow cells in individual experiments. *$P < 0.01$. (**g–i**) T cell proliferation in DC–T cell cocultures using *Tnf*$^{-/-}$, *Nfkbia*$^{-/-}$*Tnf*$^{-/-}$ and *Nfkbia*$^{-/-}$*Tnf*$^{-/-}$*Relb*$^{-/-}$ BMDCs exposed to medium (**g**), OVA peptide (**h**) or OVA protein (**i**). Top, raw FACS data of CFSE-labeled T cells stained for IL-2, showing proliferation-associated dye dilution and IL-2 production. Middle, fraction of divided cells and, bottom, fraction of T cells positive for the indicated activation-associated cytokine, graphed as a function of the DC:T cell ratio. Data in **a**,**b**,**d**,**e** are representative of at least two independent experiments. Data in **g–i** are the average of duplicate leukocyte reactions produced for each of two independent BMDC cultures. Error bars, s.e.m.; $n = 4$.

nuclear localization. Then we destabilized p100 by the IKK1-dependent pathway to achieve comparable p100 expression as in MEFs (**Fig. 1c**). This change resulted in a substantial increase of nuclear RelB activity (**Fig. 1e**). To test experimentally whether RelB in DCs primarily localizes into the nucleus, we separated BMDCs into cytoplasmic and nuclear extracts but found that more than 75% of the total RelB protein was cytoplasmic (**Fig. 1f** and **Supplementary Fig. 1c**,**d**). Indeed, whereas RelB was more abundant in the cytoplasm of BMDCs than of MEFs or BMDMs, p100 was not (**Fig. 1g**). The fact that the mathematical model, which encodes the known mechanisms of RelB control, did not reproduce our experimental observations suggested that there may be as-yet undescribed regulatory mechanisms that sequester RelB in the cytoplasm.

IκBα restrains RelB-p50 and spontaneous DC maturation

To search for inhibitors of RelB in DCs, we immunoprecipitated RelB from BMDC whole-cell lysates and analyzed the associated proteins (**Fig. 2a**). As expected, p100, the known RelB inhibitor and noncanonical regulator, was associated with RelB. Unexpectedly, IκBα and IκBε, the classical IκB inhibitors regulating the canonical NF-κB pathway, were also immunoprecipitated with RelB, but IκBβ and p105 were not. Substantial amounts of p50, known as the binding partner of RelA in the canonical pathway, were found in RelB immunoprecipitates, and this complex was primarily cytoplasmic (**Supplementary Fig. 2a**,**b**). Reciprocal immunoprecipitation of various NF-κB inhibitors confirmed that RelB not only directly interacted with p100 but also associated with IκBα and IκBε in BMDCs (**Fig. 2b** and **Supplementary Fig. 2c**), and RelA associated with IκBα, as expected (**Supplementary Fig. 2d**). The observations that IκB immunoprecipitates did not contain other IκB isoforms confirmed the specificity of the antibodies used and that only one IκB isoform associated with each RelB molecule. Analyses of the amounts of RelB captured and remaining in the flow-through after immunoprecipitation with various IκB antibodies provides a quantitative understanding of RelB protein distribution in BMDCs (**Fig. 2c**). This analysis revealed that 37–45% of RelB was associated with p100 and 12–17% with IκBε. A substantial proportion of RelB (19–34%) associated with IκBα, which prompted us to investigate the function of this interaction.

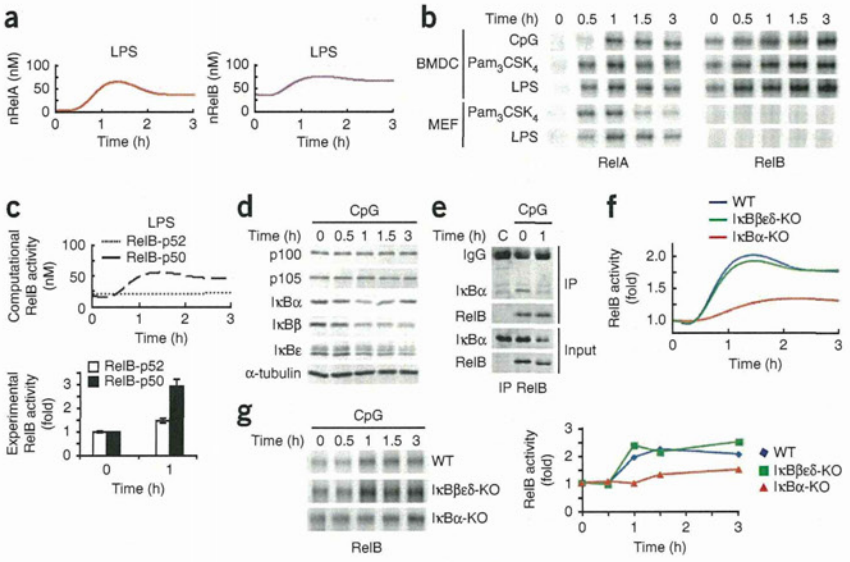

Figure 3 RelB-p50 is rapidly activated during TLR-mediated DC maturation. (**a**) Computational simulations of LPS-induced RelA and RelB activity during a 3 h time course using the refined mathematical model version 5.1–DC. (**b**) NF-κB RelA (left) and NF-κB RelB (right) DNA binding activities monitored by EMSA. Nuclear extracts from wild-type (WT) BMDCs or WT MEFs activated by indicated stimuli were collected and subjected to EMSA. Equal amounts of nuclear proteins from BMDCs or MEFs were loaded and exposure of images was adjusted to reveal similar RelA peak activity in BMDCs and MEFs. (**c**) Computational simulations of RelB-p50 and RelB-p52 activities upon LPS stimulation that sum up to total nuclear RelB activity shown in **a** (top). Quantification of RelB-p50 and RelB-p52 activities before and after CpG stimulation relative to their respective basal activity (bottom). (**d**) IκB protein expression profiles induced by CpG. Whole-cell extracts prepared from WT BMDCs were subjected to immunoblotting with antibodies to indicated proteins. (**e**) Association of IκBα to RelB monitored during a CpG time course by examining RelB immunoprecipitates (IP) from CpG-stimulated WT BMDCs. Immunoprecipitation with *Relb*$^{-/-}$ extracts (C) serves as a control, indicating specificity of RelB antibody. (**f**) Computational simulations of CpG-induced RelB activation in mathematical models, based on version 5.1–DC that were deficient (KO) in the indicated proteins. (**g**) CpG-induced NF-κB RelB DNA binding activities in BMDCs depleted for indicated proteins by knockout (KO), monitored by EMSA (left). Signals were quantified and graphed relative to respective resting cells (right). Data shown in **b**,**d**,**e**,**g** are representative of at least three independent experiments. Data shown in **c** are representative of two independent experiments (error bars, s.d.; $n = 3$).

To test whether IκBα may inhibit RelB activity in BMDCs, we took advantage of IκBα-deficient mice[22] and developed two strategies to focus our experimental analysis on RelB activity. First, we bred the mice onto a c-Rel–deficient background (*Rel*$^{-/-}$); then we modified the standard electrophoretic mobility shift assay (EMSA) with κB site–containing probes (κB EMSA) to include shift-ablating antibodies for RelA, resulting in a specific RelB EMSA. Using these tools, we found that RelB activity was more than twofold elevated in IκBα-deficient BMDCs (**Fig. 2d**). Supershift analysis with antibodies that were shown to be specific for p50 and p52 (**Supplementary Fig. 2e**) revealed that whereas control BMDCs contained primarily constitutive RelB-p52 activity, ablation of IκBα resulted in a substantial increase in active RelB-p50 dimer, rendering RelB-p50 the predominant NF-κB activity in IκBα-deficient BMDCs (**Fig. 2e**). We examined the functional consequences of RelB misregulation by monitoring the frequency of matured DCs as indicated by surface expression of the activation markers CD86 and MHC II. IκBα deficiency resulted in an increased percentage (42% versus 28%) of MHCII^{hi}CD86^{hi} BMDCs in the absence of external stimuli (**Fig. 2f**). Although RelB deficiency did not affect the frequency of MHCII^{hi}CD86^{hi} BMDCs before exposure to maturation stimuli (**Supplementary Fig. 2f**), the inappropriate spontaneous DC maturation phenotype of IκBα-deficient BMDCs was dependent on RelB, as compound deletion of the *Relb* gene fully reversed the phenotype (**Fig. 2f**). We then examined the antigen-presenting functions of DCs by testing their ability to activate proliferation and cytokine production of antigen-specific T cells in DC–T cell cocultures (**Fig. 2g–i**). We found that IκBα deficiency increased the antigen-presenting functions in BMDC cocultures with ovalbumin (OVA)-responsive T cells exposed to OVA peptide, and this effect was largely but not entirely dependent on RelB (**Fig. 2h**), correlating with the partial dependence on RelB of surface MHC expression (**Fig. 2f**). However, when we exposed these cocultures to ovalbumin protein, which must be taken up and processed before being presented, T cell activation showed a near absolute dependence on RelB (**Fig. 2i**), correlating with previous studies of RelB-deficient DCs[6], and suggesting a specific function for RelB in regulating the antigen uptake and processing program of antigen-presenting cells. Together, these data demonstrate that the classical NF-κB inhibitor, IκBα, not only restrains the expression of RelB by controlling RelA or c-Rel[24], but in immature DCs it also has a critical functional role in restraining RelB activity to prevent inappropriate spontaneous maturation.

TLRs activate RelB-p50 via the canonical NFκB pathway

To explore the regulatory consequences of RelB-p50 interactions with IκBα and IκBε proteins during DC maturation, we incorporated them into the mathematical model as kinetic rate equations and used the quantitative immunoprecipitation results as constraints in a multidimensional parameter optimization protocol (**Supplementary Note**). We simulated NF-κB regulation during Toll-like receptor (TLR)-induced DC maturation using experimentally measured time-course data of the NEMO-dependent IKK kinase activity as an input. Such simulations indicated rapid and substantial activation not only of RelA but also of RelB (**Fig. 3a**). To test this prediction experimentally, we stimulated BMDCs and MEFs with the TLR9 ligand CpG, the TLR2 ligand Pam_3CSK_4 and the TLR4 ligand LPS as well as an agonistic antibody to LTßR to induce the noncanonical NF-κB pathway. To specifically examine the activation profiles of RelA-containing and RelB-containing NF-κB dimers, we used the newly developed RelA EMSA[22] and RelB EMSA using shift-ablating antibodies for activation domain–containing Rel proteins (**Supplementary Fig. 3b**). RelA activation was similar in BMDCs and MEFs stimulated with TLR ligands (**Fig. 3b**). We observed rapid RelB activation in response to TLR stimuli in BMDCs but not in MEFs, although MEFs activated RelB at later time points when stimulated with anti-LTßR (**Fig. 3b** and **Supplementary Fig. 3c**). Similarly, we

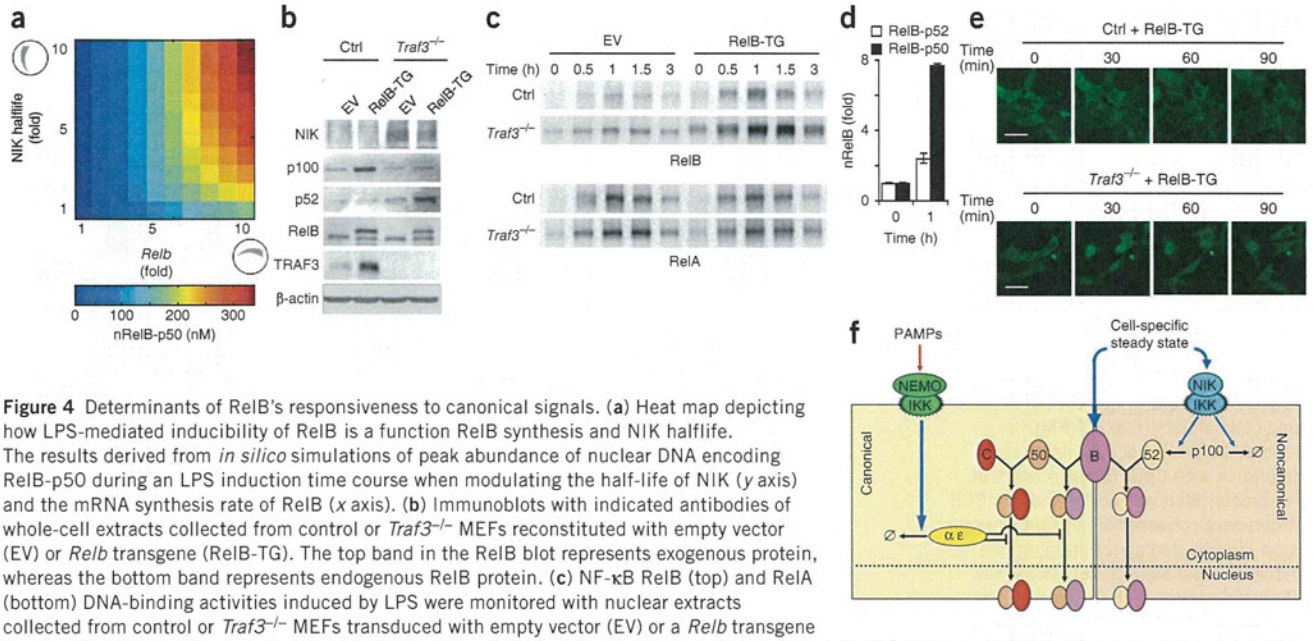

Figure 4 Determinants of RelB's responsiveness to canonical signals. (**a**) Heat map depicting how LPS-mediated inducibility of RelB is a function RelB synthesis and NIK halflife. The results derived from *in silico* simulations of peak abundance of nuclear DNA encoding RelB-p50 during an LPS induction time course when modulating the half-life of NIK (*y* axis) and the mRNA synthesis rate of RelB (*x* axis). (**b**) Immunoblots with indicated antibodies of whole-cell extracts collected from control or *Traf3*$^{-/-}$ MEFs reconstituted with empty vector (EV) or *Relb* transgene (RelB-TG). The top band in the RelB blot represents exogenous protein, whereas the bottom band represents endogenous RelB protein. (**c**) NF-κB RelB (top) and RelA (bottom) DNA-binding activities induced by LPS were monitored with nuclear extracts collected from control or *Traf3*$^{-/-}$ MEFs transduced with empty vector (EV) or a *Relb* transgene (RelB-TG). (**d**) Quantification of nuclear (n)RelB-p50 and RelB-p52 activities in LPS-stimulated *Traf3*$^{-/-}$ (*Relb* transgene) MEFs; signals were graphed relative to respective RelB-containing dimers' basal activity. (**e**) Single-cell data at indicated time points[7] of the nuclear localization of a retrovirally expressed RelB-GFP fusion protein in response to TNF stimulation of control or *Traf3*$^{-/-}$ MEFs (RelB-TG). Scale bars, 10 μm. (**f**) Schematic depicting the regulation of RelB by noncanonical or canonical stimuli. RelB may either dimerize with p52 in response to stimulus-induced noncanonical stimuli or dimerize with p50 and become responsive to canonical stimuli. Cell type–specific steady-state control of RelB expression and noncanonical pathway activity determines which stimuli activate RelB: at low steady-state levels, RelB is responsive to noncanonical stimuli as reported in MEFs; at high steady-state levels RelB will dimerize not only p52 but also p50, and becomes responsive to canonical stimuli via IκBα and IκBε control. Data shown here are representative of two independent experiments (error bars, s.d.; $n = 3$).

observed rapid activation of RelB in splenic DCs stimulated with CpG or Pam_3CSK_4 (**Supplementary Fig. 3d**). Computational simulations suggested that this induced RelB activity consists of RelB-p50 rather than RelB-p52 dimer (**Fig. 3c**). Experimentally, supershift analyses of nuclear extracts revealed that both RelB-p50 and RelB-p52 activities were present under unstimulated conditions but that CpG stimulation primarily increased RelB-p50 activity (**Fig. 3c** and **Supplementary Fig. 3e**), unlike LTßR stimulation of MEFs, which induces RelB-p52. These data suggest that during DC maturation RelB activation is regulated by the canonical pathway.

A hallmark of canonical signaling is the release of a pre-existing NF-κB dimer, whereas noncanonical signaling involves the stimulus-responsive *de novo* generation of the dimer[12,25]. In CpG-responding DCs we did not detect increases in protein expression of RelB or p50, or *Relb* mRNA, whereas *Nfkbia* mRNA, encoding IκBα, was induced more than fourfold (**Supplementary Fig. 3f**). Furthermore, inhibition of protein synthesis by cycloheximide did not block CpG-induced RelB activation, whereas resynthesis of IκBα protein was blocked (**Supplementary Fig. 3g**), suggesting that *de novo* RelB protein synthesis is not required for CpG-inducible RelB activation. In contrast, immunoblotting confirmed that in DCs nuclear accumulation of RelB was accompanied by disappearance of cytoplasmic RelB after CpG stimulation, indicative of stimulus-responsive nuclear translocation of a pre-existing pool of RelB (**Supplementary Fig. 3h**). Inhibition of IKK2 activity, a hallmark of the canonical pathway, by the inhibitor PS-1145 (ref. 26) resulted not only in reduced RelA activity and IκBα protein degradation but also in reduced RelB activation (**Supplementary Fig. 3g,i**), suggesting that IKK2 signaling is required for RelB activation. We monitored the abundance of known NF-κB inhibitor proteins during the CpG time course: the abundance of the potential RelB inhibitors p100 and p105 remained unaltered; however, IκBα and IκBε were rapidly degraded, correlating with the activation kinetics of RelB activation (**Fig. 3d**). Notably, in coimmunoprecipitation assays, the amount of IκBα associated with RelB decreased in response to CpG (**Fig. 3e**). Together, these data suggest that degradation of IκBα allows for the release of RelB from pre-existing IκBα-RelB complexes.

To investigate the role of IκBα in TLR-induced RelB activation, we used the mathematical model to computationally simulate the effect of IκB deletions on RelB activation. We found that *in silico* deletion of individual inhibitors had little effect, except in the case of IκBα (**Supplementary Fig. 3j**). Even compound deficiency of IκBβ, IκBε and IκBδ (which elevated basal RelB activity; **Supplementary Fig. 3k**) showed robust RelB activation in response to canonical pathway activation, as opposed to greatly diminished activation in an IκBα-deficient model (**Fig. 3f**). To test these computational modeling predictions, we used IκBα-deficient mice[22] and generated *Nfkbib*$^{-/-}$*Nfkbie*$^{-/-}$*Nfkb2*$^{-/-}$ mice. We confirmed the lack of protein products by immunoblotting (**Supplementary Fig. 3l**). Indeed, RelB activation was robust in *Nfkbib*$^{-/-}$*Nfkbie*$^{-/-}$*Nfkb2*$^{-/-}$ BMDCs, whereas IκBα-deficient BMDCs showed a diminished increase and delayed kinetics (**Fig. 3g** and **Supplementary Fig. 3m**). Together, these data provide genetic and mechanistic evidence that IκBα is required for CpG-induced RelB activation in DCs.

Engineered MEFs show DC-like RelB control

We previously showed that hallmarks of the NF-κB signaling system in mature but unstimulated DCs are abundant in basal RelB expression

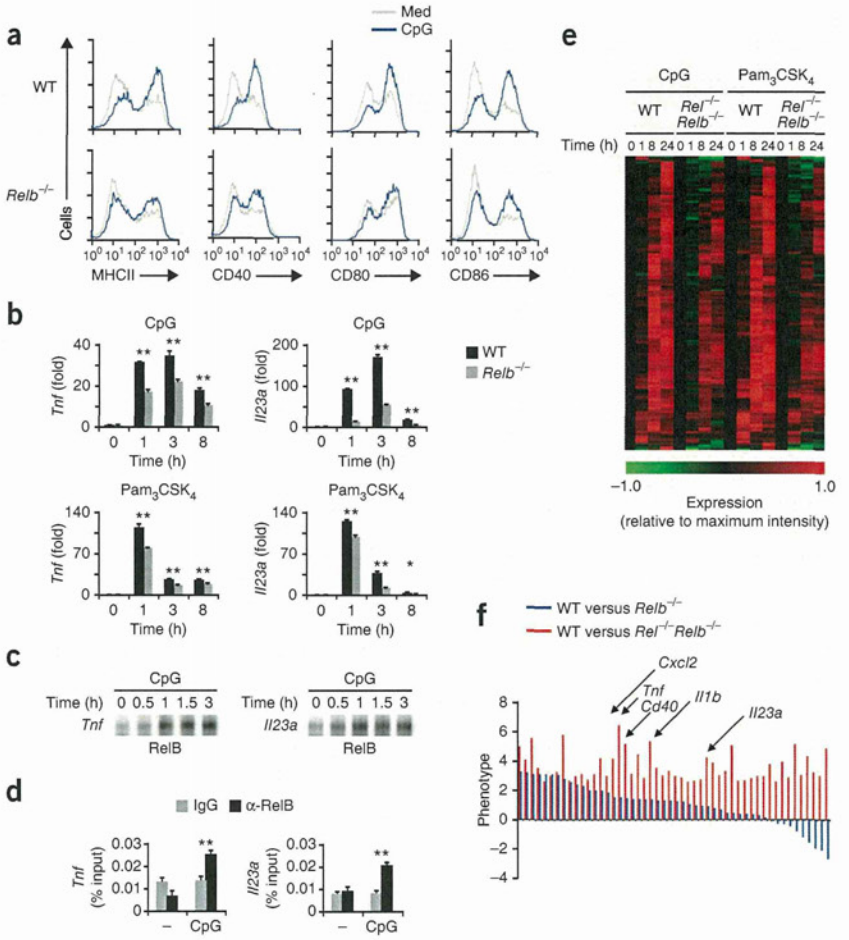

Figure 5 RelB regulates DC activation markers and inflammatory mediators. (**a**) Analysis of cell surface marker expression in wild-type (WT) and *Relb*$^{-/-}$ BMDCs in response to CpG. Cells untreated (Med) or treated with CpG for 24 h were analyzed by FACS. (**b**) Gene expression analyses of WT and *Relb*$^{-/-}$ BMDCs stimulated with CpG or Pam_3CSK_4 for the indicated time course by qRT-PCR. Signals were graphed relative to respective resting cells. (**c**) EMSA with nuclear extracts collected from CpG-stimulated WT BMDCs using DNA probes containing the κB site containing promoter sequence from *Tnf* or *Il23a* gene. (**d**) Chromatin immunoprecipitation analyses with RelB or IgG control antibodies using cell extracts from WT BMDCs collected before (–) or 75 min after stimulation with CpG. Quantification of DNA precipitated was performed by qPCR with primers corresponding to the promoter region of indicated genes and graphed relative to input signals. (**e**) Microarray mRNA expression analysis from WT and *Rel*$^{-/-}$*Relb*$^{-/-}$ BMDCs stimulated with CpG and Pam_3CSK_4 for indicated time points. Heat map shows the expression pattern from one experiment in a (log_2) fold induction scale of 157 significant downregulated genes in *Rel*$^{-/-}$*Relb*$^{-/-}$ BMDCs identified by significant analysis of microarray (SAM). Color scale '1.0' denotes normalized highest expression value of the given gene across time courses. (**f**) RelB and c-Rel regulate overlapping sets of genes. The expression phenotype caused by RelB deficiency was determined for the 50 genes with the most severe expression defect in *Rel*$^{-/-}$*Relb*$^{-/-}$ BMDCs. The list of genes was sorted according to expression differences between WT and *Relb*$^{-/-}$ BMDCs. Data shown in **a**–**d** are representative of at least three independent experiments (error bars, s.e.m.; $n = 3$). $^*P < 0.05$ and $^{**}P < 0.01$.

and basal noncanonical pathway activity. To investigate whether these mechanisms are sufficient and what their relative contributions may be, we performed computational simulations of RelB activation for a range of parameter values governing basal *Relb* mRNA synthesis and NIK protein half-life. These *in silico* analyses showed that activation of RelB mildly increased when either parameter was increased, but substantial enhancement occurred only when both parameters were concomitantly elevated (**Fig. 4a**). Our simulations suggest that the DC-specific, rapid RelB activation upon canonical pathway stimulation can be explained by DC-specific, constitutively elevated *Relb* mRNA synthesis and noncanonical IKK activity.

To test this model-derived hypothesis experimentally, we asked whether genetically engineering these two mechanisms into MEFs may be sufficient to allow for DC-like canonical regulation of RelB. We took advantage of MEFs deficient in TRAF3, an E3-ligase controlling NIK degradation[27], to increase constitutive noncanonical signaling. As suggested by the model simulations, we then transduced a retroviral *Relb* transgene to increase RelB expression about threefold relative to that in untransduced MEFs (**Fig. 4b** and **Supplementary Fig. 4a**). The engineered MEFs exhibited substantial RelB activation in response to LPS (**Fig. 4c**) or TNF (**Supplementary Fig. 4b**), whereas the parental control MEFs did not, and RelA activation by these stimuli remained unchanged. Neither single genetic alteration produced substantial RelB activation, indicating that enhanced RelB expression and noncanonical pathway activity function synergistically, as predicted by the model, to push RelB into the canonical pathway and render it responsive to TLR agonists. Antibody supershift and depletion analysis (**Fig. 4d** and **Supplementary Fig. 4c**) confirmed that canonical signaling primarily activated the RelB-p50 dimer (sevenfold) rather than the RelB-p52 dimer (twofold) as observed in DCs and predicted by the computational model (**Fig. 3c**). Overexpression of a RelB-GFP fusion protein retrovirally transduced into single cells also revealed nuclear translocation upon TNF stimulation in the *Traf3*$^{-/-}$ context but not in control cells (**Fig. 4e**).

These iterative computational-experimental studies support a model in which the NF-κB protein RelB may function in either noncanonical or canonical pathways (**Fig. 4f**). In a dimer with p100 or p52, RelB is subject to control by the noncanonical pathway; in a dimer with p50, RelB may be bound by IκBα and IκBε and is regulated by NEMO-dependent canonical signals. Our analysis indicates that low constitutive RelB expression and noncanonical pathway activity characterizes one steady state (found in MEFs) and allows for RelB-p52 activation by stimuli such as LTβ that engage the noncanonical pathway (**Supplementary Fig. 4d**). High constitutive RelB expression and noncanonical pathway activity characterize another steady state (found in DCs) and allow for RelB-p50 activation by stimuli such as CpG that engage the canonical pathway (**Supplementary Fig. 4e**).

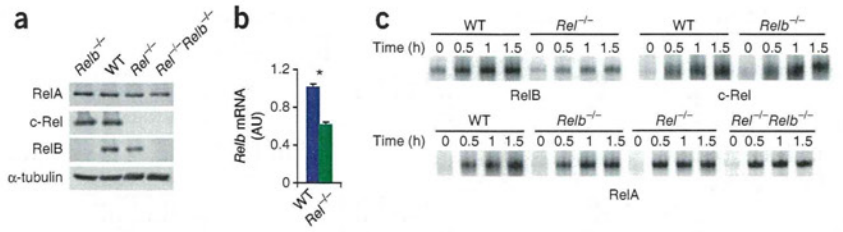

Figure 6 RelB may mediate cRel functions in DCs. (**a**) Immunoblot for RelA, RelB and c-Rel of whole-cell extracts prepared from indicated BMDCs. α-tubulin served as a loading control. (**b**) Amount of *Relb* transcripts compared by quantitative RT-PCR with mRNA collected from wild-type and *Rel*$^{-/-}$ BMDCs, relative to wild-type (WT) cells. (**c**) NF-κB DNA binding activities of RelB, c-Rel and RelA induced by LPS in indicated gene-deficient BMDCs monitored by EMSA. Data shown are representative of three independent experiments (error bars, s.e.m.; $n = 4$). *$P < 0.01$.

RelB and c-Rel cooperate in TLR-induced DC maturation

Given that RelB-p50 is induced by PAMPs during DC maturation, we wondered whether it controls the expression of inflammatory regulators or DC activation markers. After stimulation with the TLR9 ligand CpG or the TLR2 ligand Pam_3CSK_4 for 24 h, we indeed observed reduced surface expression of DC activation markers MHCII, CD86, CD80 and CD40 in *Relb*$^{-/-}$ DCs (**Fig. 5a** and **Supplementary Fig. 5a,b**). Expression of proinflammatory genes, *Tnf* and *Il23a*, correlated with the kinetics of CpG or Pam_3CSK_4-induced RelB activation and were reduced in *Relb*$^{-/-}$ DCs (**Fig. 5b**). In EMSAs, activated RelB-p50 bound to DNA probes containing the κB sites found in the *Tnf* and *Il23a* promoters (**Fig. 5c**), indicating that RelB-p50 can directly interact with these regulatory regions. *In vivo*, we observed recruitment of RelB to the promoter regions of *Tnf* and *Il23a* genes after DC maturation with CpG using the chromatin immunoprecipitation assay (**Fig. 5d**).

We noted that RelB bound to consensus κB site sequences[28] associated with the known canonical NF-κB pathway effectors, RelA and c-Rel, rather than the unconventional sequences previously ascribed to RelB in splenic stromal cells[29] or MEFs[20]. Because single knockouts did not show overt defects in CD11c$^+$ cell generation in bone marrow cultures (**Supplementary Fig. 5d**), we tested whether c-Rel and RelB have overlapping functions in regulating the DC maturation program by examining gene expression in c-Rel and RelB doubly-deficient DCs. Genome-wide expression profiling activated by TLR ligands CpG and Pam_3CSK_4 revealed a group of 157 genes that were substantially downregulated in *Rel*$^{-/-}$*Relb*$^{-/-}$ BMDCs (**Fig. 5e** and **Supplementary Table 1**). To delineate the contribution of RelB in activating these genes, we examined the expression phenotype of the 50 most severely c-Rel–RelB-dependent genes in *Relb*$^{-/-}$ BMDCs stimulated with TLR ligands. Expression phenotypes in fold induction were calculated between wild-type and null DCs, and the order of genes was sorted in increasing degree of RelB dependency (**Fig. 5f** and **Supplementary Table 2**). This analysis revealed a continuous spectrum of RelB dependency rather than two distinct classes (of RelB-dependent and RelB-independent genes), suggesting an overlap in DNA interaction specificities between c-Rel and RelB dimers. *Tnf* and *Il23a* were identified in this analysis as regulated by both RelB and c-Rel. Quantitative RT-PCR validated the requirements of RelB and c-Rel in activating *Cxcl2*, *Cd40* and *Il1b* gene expression (**Supplementary Fig. 5c**).

Given overlapping functions of c-Rel and RelB in regulating DC gene expression programs, we investigated their relationship within the signaling system. Whereas RelA and c-Rel protein expression were similarly abundant in wild-type BMDCs and those lacking RelB, *Rel*$^{-/-}$ BMDCs exhibited decreased RelB protein expression (**Fig. 6a**). *Relb* transcripts were reduced by ~40% in *Rel*$^{-/-}$ relative to wild-type BMDC (**Fig. 6b**). This reduction resulted in severely diminished activation of RelB DNA-binding activity in *Rel*$^{-/-}$ BMDCs in response to LPS (**Fig. 6c**). These data indicate that one of the key determinants of RelB control by the canonical pathway, namely RelB expression, is in fact controlled by c-Rel. The feed-forward circuit architecture suggests that expression of RelB in differentiated but immature DCs may reflect the exposure of differentiating cells to c-Rel–inducing stimuli. We therefore tested whether c-Rel–deficient DCs may also be defective in RelB-responsive gene expression by comparing the expression of RelB target genes in *Rel*$^{-/-}$ DCs and *Rel*$^{-/-}$*Relb*$^{-/-}$ DCs. Indeed, *Rel*$^{-/-}$ BMDCs showed reductions of surface marker and inflammatory cytokine expression (**Supplementary Fig. 6a,b**). These data support a model in which RelB acts as a downstream mediator of c-Rel in DC activation programs.

DISCUSSION

RelA and c-Rel had been previously considered as effectors of the canonical NF-κB signaling pathway, and RelB as the effector of the noncanonical pathway, based on its role as a RelB-p52 transcription factor in secondary lymphoid organogenesis. However, we showed here that RelB is also an effector of the canonical pathway in DCs. During DC differentiation RelB expression increased, and elevated steady-state noncanonical pathway activity resulted not only in the expected RelB-p52 dimer but in formation of the RelB-p50 dimer. Unlike RelB-p52, which is mostly nuclear in immature DCs, RelB-p50 is inhibited by the IκB proteins, IκBα and IκBε, which allows for rapid activation of RelB-p50 activity via the canonical pathway upon exposure to maturation stimuli. Conversely, with the recent discovery of IκBδ[21,22], chronic inflammatory conditions rendered RelA an effector of the noncanonical signaling pathway. Thus, both RelA and RelB are potential effectors of the canonical and noncanonical signaling pathways; whether they are functionally relevant effectors is determined by the physiological steady state of the NF-κB signaling system.

Our observations imply that RelB-p50 and RelB-p52 present different molecular surfaces to IκB proteins, providing physiological relevance to previous studies of protein-interaction specificities[30,31]. Similarly, the DNA interaction characteristics of RelB-p50 and RelB-p52 may be distinct[32,33]. RelB residue Arg125 in the RelB-p52 dimer makes an additional base contact with DNA that allows RelB-p52 to recognize a broader range of κB sites. This may account for the RelB-p52–specific function in regulating chemokines involved in secondary lymphoid organogenesis, such as secondary lymphoid tissue chemokine (SLC), EBI1 ligand chemokine (ELC), B lymphoblastoid cell chemokine (BLC) and stromal cell–derived factor 1α (SDF-1α)[20,29]. In contrast, RelB-p50 interacts with DNA sequences similarly to RelA-p50, and a role for RelB in TNF production, GM-CSF and Bcl-xl expression has been reported[34,35]. Together, these studies suggest that the dimerization partner of RelB determines not only the signaling pathway that RelB is responsive to but also the RelB target gene program.

Why then, would DCs use RelB as an effector of the canonical NF-κB signaling pathway along with RelA and c-Rel? One possibility

is that RelB-p50 target genes are distinct from those controlled by c-Rel or RelA. Our transcriptomic profiling suggests overlap between c-Rel–dependent and RelB-dependent gene programs, but c-Rel turned out to control RelB expression; thus, other tools are required to address the question of RelB-p50 versus cRel-p50 specificity. A second possibility is that the stimulus-responsive dynamic control of RelB is distinct from that of RelA or c-Rel. Although RelB-p50 is inhibited by IκBα in resting cells, it may make for a poorer substrate for IκB feedback control than RelA, which is efficiently stripped off the DNA by IκBα[36]. We speculate that the involvement of RelB-p50 in DC biology ensures irreversible execution of a terminal maturation and activation program in response to transient PAMP exposure.

Mathematical modeling, which we used here to describe biochemical reactions in terms of kinetic rate equations, lends itself as a tool for studying the regulation of signaling networks. Iteratively refined mathematical models of the NF-κB–IκB system have addressed the dynamic and homeostatic control of the NF-κB RelA-p50 dimer by IκB proteins in fibroblasts[21,22,37–41]. In this study, we developed to our knowledge the first kinetic model that accounts for the generation and regulation of multiple NF-κB dimers, namely RelA- and RelB- containing dimers. We contrasted the steady-state and dynamic control mechanisms in two cell types, MEFs and DCs, and found that the key biochemical differences are two kinetic rate constants (*Relb* mRNA synthesis and NIK half-life); a threefold increase was sufficient to shift the *in silico* model from MEF-like to DC-like regulation of the NF-κB signaling system. We confirmed this prediction experimentally by genetically engineering MEFs to produce DC-like RelB control. There was no need to invoke cell type–specific protein interaction specificities or any other cell type–specific molecular mechanism. The results indicate that cell type–specific quantitative control of the steady state of a signaling system may determine seemingly qualitative cell type–specific properties, such as DC-specific RelB activation by TLRs. As such, kinetic modeling and a quantitative analysis of signaling systems may serve to generate hypotheses not only for mechanistic studies but also for the development of DC-mediated therapeutics.

METHODS

Methods and any associated references are available in the online version of the paper.

Accession codes. GEO: microarray data, GSE34990.

Note: Supplementary information is available in the online version of the paper.

ACKNOWLEDGMENTS

We thank Z. Tao and G. Ghosh (University of California San Diego) for plasmids and recombinant proteins, S. Basak, A. Wu, P. Loriaux, R. Tsui for computational modeling advice, and C. Brown and M. Karin (University of California San Diego) for *Traf3*$^{-/-}$ embryos. This study was supported by GM085763 (A.H.), GM071573 (A.H.), AI090935 (A.H.), GM085325 (J.P.) and AI081923 (E.I.Z.).

AUTHOR CONTRIBUTIONS

V.F.-S.S. and A.H. designed the study. V.F.-S.S. and M.M. carried out all experimental work with assistance from J.Q.H., T.Y., R.F. and M.A., and guidance from E.I.Z. and A.H. J.D.-T. and J.D.K. carried out the computational modeling work and J.P. the bioinformatic analysis. V.F.-S.S. and A.H. wrote the manuscript with contributions from all authors.

COMPETING FINANCIAL INTERESTS

The authors declare no competing financial interests.

Published online at http://www.nature.com/doifinder/10.1038/ni.2446.
Reprints and permissions information is available online at http://www.nature.com/reprints/index.html.

1. Banchereau, J. & Steinman, R.M. Dendritic cells and the control of immunity. *Nature* **392**, 245–252 (1998).
2. Liu, Y.J. IPC: professional type 1 interferon-producing cells and plasmacytoid dendritic cell precursors. *Annu. Rev. Immunol.* **23**, 275–306 (2005).
3. Serbina, N.V., Salazar-Mather, T.P., Biron, C.A., Kuziel, W.A. & Pamer, E.G. TNF/iNOS-producing dendritic cells mediate innate immune defense against bacterial infection. *Immunity* **19**, 59–70 (2003).
4. Steinman, R.M. & Banchereau, J. Taking dendritic cells into medicine. *Nature* **449**, 419–426 (2007).
5. Carrasco, D., Ryseck, R.P. & Bravo, R. Expression of relB transcripts during lymphoid organ development: specific expression in dendritic antigen-presenting cells. *Development* **118**, 1221–1231 (1993).
6. Zanetti, M., Castiglioni, P., Schoenberger, S. & Gerloni, M. The role of relB in regulating the adaptive immune response. *Ann. NY Acad. Sci.* **987**, 249–257 (2003).
7. Li, M. *et al.* Immune modulation and tolerance induction by RelB-silenced dendritic cells through RNA interference. *J. Immunol.* **178**, 5480–5487 (2007).
8. Wu, L. *et al.* RelB is essential for the development of myeloid-related CD8α- dendritic cells but not of lymphoid-related CD8α+ dendritic cells. *Immunity* **9**, 839–847 (1998).
9. Kobayashi, T. *et al.* TRAF6 is a critical factor for dendritic cell maturation and development. *Immunity* **19**, 353–363 (2003).
10. Hofmann, J., Mair, F., Greter, M., Schmidt-Supprian, M. & Becher, B. NIK signaling in dendritic cells but not in T cells is required for the development of effector T cells and cell-mediated immune responses. *J. Exp. Med.* **208**, 1917–1929 (2011).
11. Yang, H. *et al.* Suppression of ongoing experimental autoimmune myasthenia gravis by transfer of RelB-silenced bone marrow dentritic cells is associated with a change from a T helper Th17/Th1 to a Th2 and FoxP3+ regulatory T-cell profile. *Inflamm. Res.* **59**, 197–205 (2010).
12. Pomerantz, J.L. & Baltimore, D. Two pathways to NF-κB. *Mol. Cell* **10**, 693–695 (2002).
13. Oeckinghaus, A., Hayden, M.S. & Ghosh, S. Crosstalk in NF-κB signaling pathways. *Nat. Immunol.* **12**, 695–708 (2011).
14. Derudder, E. *et al.* RelB/p50 dimers are differentially regulated by tumor necrosis factor-alpha and lymphotoxin-beta receptor activation: critical roles for p100. *J. Biol. Chem.* **278**, 23278–23284 (2003).
15. Lind, E.F. *et al.* Dendritic cells require the NF-κB2 pathway for cross-presentation of soluble antigens. *J. Immunol.* **181**, 354–363 (2008).
16. O'Sullivan, B.J. & Thomas, R. CD40 ligation conditions dendritic cell antigen-presenting function through sustained activation of NF-κB. *J. Immunol.* **168**, 5491–5498 (2002).
17. Saccani, S., Pantano, S. & Natoli, G. Modulation of NF-κB activity by exchange of dimers. *Mol. Cell* **11**, 1563–1574 (2003).
18. Ammon, C., Mondal, K., Andreesen, R. & Krause, S.W. Differential expression of the transcription factor NF-κB during human mononuclear phagocyte differentiation to macrophages and dendritic cells. *Biochem. Biophys. Res. Commun.* **268**, 99–105 (2000).
19. Gasparini, C., Foxwell, B.M. & Feldmann, M. RelB/p50 regulates CCL19 production, but fails to promote human DC maturation. *Eur. J. Immunol.* **39**, 2215–2223 (2009).
20. Basak, S., Shih, V.F. & Hoffmann, A. Generation and activation of multiple dimeric transcription factors within the NF-κB signaling system. *Mol. Cell. Biol.* **28**, 3139–3150 (2008).
21. Basak, S. *et al.* A fourth IκB protein within the NF-κB signaling module. *Cell* **128**, 369–381 (2007).
22. Shih, V.F. *et al.* Kinetic control of negative feedback regulators of NF-κB/RelA determines their pathogen- and cytokine-receptor signaling specificity. *Proc. Natl. Acad. Sci. USA* **106**, 9619–9624 (2009).
23. Li, T. *et al.* MicroRNAs modulate the noncanonical transcription factor NF-κB pathway by regulating expression of the kinase IKKα during macrophage differentiation. *Nat. Immunol.* **11**, 799–805 (2010).
24. Wuerzberger-Davis, S.M. *et al.* Nuclear export of the NF-κB inhibitor IκBα is required for proper B cell and secondary lymphoid tissue formation. *Immunity* **34**, 188–200 (2011).
25. Shih, V.F., Tsui, R., Caldwell, A. & Hoffmann, A. A single NFκB system for both canonical and non-canonical signaling. *Cell Res.* **21**, 86–102 (2011).
26. Waterfield, M., Jin, W., Reiley, W., Zhang, M. & Sun, S.C. IκB kinase is an essential component of the Tpl2 signaling pathway. *Mol. Cell. Biol.* **24**, 6040–6048 (2004).
27. He, J.Q. *et al.* Rescue of TRAF3-null mice by p100 NF-κB deficiency. *J. Exp. Med.* **203**, 2413–2418 (2006).
28. Hoffmann, A., Natoli, G. & Ghosh, G. Transcriptional regulation via the NF-κB signaling module. *Oncogene* **25**, 6706–6716 (2006).
29. Bonizzi, G. *et al.* Activation of IKKα target genes depends on recognition of specific κB binding sites by RelB:p52 dimers. *EMBO J.* **23**, 4202–4210 (2004).
30. Lernbecher, T., Kistler, B. & Wirth, T. Two distinct mechanisms contribute to the constitutive activation of RelB in lymphoid cells. *EMBO J.* **13**, 4060–4069 (1994).
31. Dobrzanski, P., Ryseck, R.P. & Bravo, R. Differential interactions of Rel-NF-κB complexes with IκBα determine pools of constitutive and inducible NF-κB activity. *EMBO J.* **13**, 4608–4616 (1994).

32. Fusco, A.J. *et al.* NF-κB p52:RelB heterodimer recognizes two classes of κB sites with two distinct modes. *EMBO Rep.* **10**, 152–159 (2009).
33. Moorthy, A.K., Huang, D.B., Wang, V.Y., Vu, D. & Ghosh, G. X-ray structure of a NF-κB p50/RelB/DNA complex reveals assembly of multiple dimers on tandem κB sites. *J. Mol. Biol.* **373**, 723–734 (2007).
34. Weih, F., Warr, G., Yang, H. & Bravo, R. Multifocal defects in immune responses in RelB-deficient mice. *J. Immunol.* **158**, 5211–5218 (1997).
35. Sasaki, C.Y., Ghosh, P. & Longo, D.L. Recruitment of RelB to the Csf2 promoter enhances RelA-mediated transcription of granulocyte-macrophage colony-stimulating factor. *J. Biol. Chem.* **286**, 1093–1102 (2011).
36. Bergqvist, S. *et al.* Kinetic enhancement of NF-κBxDNA dissociation by IκBα. *Proc. Natl. Acad. Sci. USA* **106**, 19328–19333 (2009).
37. Werner, S.L., Barken, D. & Hoffmann, A. Stimulus specificity of gene expression programs determined by temporal control of IKK activity. *Science* **309**, 1857–1861 (2005).
38. O'Dea, E.L., Kearns, J.D. & Hoffmann, A. UV as an amplifier rather than inducer of NF-κB activity. *Mol. Cell* **30**, 632–641 (2008).
39. O'Dea, E.L. *et al.* A homeostatic model of IκB metabolism to control constitutive NF-κB activity. *Mol. Syst. Biol.* **3**, 111 (2007).
40. Kearns, J.D., Basak, S., Werner, S.L., Huang, C.S. & Hoffmann, A. IκBepsilon provides negative feedback to control NF-κB oscillations, signaling dynamics, and inflammatory gene expression. *J. Cell Biol.* **173**, 659–664 (2006).
41. Hoffmann, A., Levchenko, A., Scott, M.L. & Baltimore, D. The IκB-NF-κB signaling module: temporal control and selective gene activation. *Science* **298**, 1241–1245 (2002).

ONLINE METHODS

Reagents. GM-CSF and IL-4 were from Peprotech. We used 0.1 μM CpG (Invivogen), 500 ng/ml Pam3CSK4 (Invivogen), 100 ng/ml LPS (Sigma, B5:055) and 0.5 μg/ml LTßR agonist (Biogen) to stimulate cells. Cycloheximide and IKK2 inhibitor (PS-1145) were from Sigma. Antibodies to RelA (sc-372), RelB (sc-226), c-Rel (sc-70), IκBα (sc-371), IκBβ (sc-945), IκBε (sc-7155), IKK1 (sc-7606), TRAF3 (sc-6933), USF-2 (sc-861), α-tubulin (sc-5286), β-actin (sc-1615) and CD16/CD32 (sc-18867) were from Santa Cruz Biotechnology. p105/p50, p100/p52 and antibody to p100 C terminus were from US National Cancer Institute, Biological Resources Branch, Frederick, Maryland, USA. NIK antibody (4994) was from Cell Signaling. Immunoprecipitation beads and HRP-conjugated anti-rabbit secondary antibody (18-8816) were from eBioscience.

Animals and cell culture. Wild-type and gene-deficient C57BL/6 mice were maintained in specific pathogen–free condition at the University of California, San Diego. All procedures were approved by the Institutional Animal Care and Use Committee of the University of California, San Diego. *Nfkbia*$^{-/-}$*Tnf*$^{-/-}$ *Rel*$^{-/-}$ and *Nfkbia*$^{-/-}$*Tnf*$^{-/-}$ *Rel*$^{-/-}$*Relb*$^{-/-}$ mice were generated by cross-breeding *Nfkbia*$^{-/-}$*Tnf*$^{-/-}$ with *Rel*$^{-/-}$ and *Relb*$^{-/-}$ mice. *Nfkbib*$^{-/-}$*Nfkbie*$^{-/-}$*Nfkb2*$^{-/-}$ mice were generated by cross-breeding *Nfkbib*$^{-/-}$, *Nfkbie*$^{-/-}$ and *Nfkb2*$^{-/-}$ mice. *Rel*$^{-/-}$*Relb*$^{-/-}$ mice were generated by cross-breeding *Rel*$^{-/-}$ and *Relb*$^{-/-}$ mice. Primary MEFs were generated from E12.5–14.5 embryos. BMDMs and BMDCs were made from bone-marrow suspensions prepared from mouse femurs. We seeded 2×10^6 bone marrow cells on 10-cm plate and cultured them for one week with L929-conditioned DMEM to derive BMDMs or cultured them for 6–11 d with 20 ng/ml GM-CSF and 10 ng/ml IL-4 to derive BMDCs. BMDC medium was replaced on days 3, 6 and 8, and floating cells were collected and subjected to experimental analyses as previously described[42]. Typically, day 6–7 BMDCs were used to investigate TLR-induced DC maturation, and day 9–11 BMDCs for spontaneous DC maturation studies.

Splenic DC purification. Spleens were cut into small fragments and digested with collagenase D (2 mg/ml, Roche) for 30 min at 37 °C followed by incubation with 10 mM EDTA pH 8.0 for 5 min. Single-cell suspension of splenocytes were enriched for CD11c$^+$ cells by immunomagnetic cell sorting using MACS CD11c microbeads (Miltenyi Biotec) according to manufacturer's protocol.

Antibody staining and flow cytometry. Single-cell suspensions were collected and blocked with anti-mouse CD16/CD32 in PBS containing 5% FCS for 10 min. Cells were stained with 7-amino-actinomycin D (7-AAD) to exclude dead cells and indicated antibodies for DC maturation analyses. All antibodies were purchased from BD Pharmingen: anti-CD11 (HL3), anti-CD40 (3/23), anti-CD80 (16-10A1), anti-CD86 (GL-1) and anti-IA^b (AF6-120.1). Stained cells were acquired in either a FACSCalibur (BD Biosciences) or an Accuri C6 and data analysis was performed with FlowJo software.

Antigen presentation in DC–T cell cocultures. GM-CSF–derived bone marrow DCs were pulsed with 200 μg whole ovalbumin (Sigma, 5 μM OVA 323-339 (OT-II) peptide (Anaspec) or medium alone for 2 h at 37 °C. Naive CD4$^+$ T cells (5×10^4 cells/well) were obtained by negative enrichment (>90% purity; Stem Cell Technologies) from spleens of B6.Cg-Tg (*TcraTcrb*)425 Cbn/J mice transgenic for ovalbumin 323-339–specific αβTCR (Jackson Laboratory) and labeled with carboxyfluorescein succinimidyl ester (CFSE) (Sigma). DCs were washed and cultured with CFSE-labeled CD4$^+$ T cells (5×10^4 T cells/well) at the indicated DC:T cell ratios as described[43]. T cells were restimulated 72 h later with 5 μM OT-II peptide for 5 h in the presence of brefeldin A and examined for CFSE dilution and production of TNF and IL-2 by flow cytometry (BD LSRII). Data were analyzed using FlowJo software (Treestar).

Biochemical analyses. Whole cell extracts were prepared in RIPA buffer and normalized for total protein or cell numbers before immunoblot analysis. Cytoplasmic and nuclear extracts from BMDMs and BMDCs were prepared by high salt extraction buffer (Buffer A: 10 mM HEPES pH 7.9, 10 mM KCl, 0.1 mM EGDA and 0.1 mM EDTA; Buffer C: 20 mM HEPES pH 7.9, 420 mM NaCl, 1.5 mM $MgCl_2$, 0.2 mM EDTA and 25% glycerol). Immunoprecipitation-immunoblotting analysis, EMSA, chromatin immunoprecipitation were performed as previously described[21,44]. In EMSAs focusing on RelB-DNA binding activity, nuclear extracts were ablated of RelA and c-Rel–containing DNA binding activities by preincubating them with RelA and c-Rel antibodies (**Fig. 3b** and **Supplementary Fig. 3b**). Similarly, nuclear extracts were preincubated with RelB and c-Rel antibodies when RelA DNA binding activity was the focus (**Fig. 3b**). Antibody-shift ablation analysis (for RelB, p50 and p52) was performed as previously described[22] and the specificities of antibodies were confirmed (**Supplementary Fig. 2e**).

Retrovirus-mediated gene transduction. RelB- or RelB-GFP expressing pBabe-puro constructs were generated by standard methods and transfected together with pCL.Eco into 293T cells with Lipofectamine 2000 transfection reagent (Invitrogen) for 48 h. Supernatant was filtered and used to infect MEFs. Transduced cells were selected with puromycin hydrochloride (Sigma). Images were acquired with a Zeiss Axio Z1 microscope.

Gene expression analysis. RNA extraction was performed with RNAeasy Mini Kit (Qiagen). RNA was collected from one set of time-course experiments (1 h, 8 h and 24 h) using wild-type (WT), *Relb*$^{-/-}$ and *Rel*$^{-/-}$*Relb*$^{-/-}$ BMDCs stimulated with 0.1 μM CpG (Invivogen) or 500 ng/ml Pam_3CSK_4. Labeling and hybridization to the Illumina v.2 gene expression chip was performed by UCSD Biogem core facility. The raw data were preprocessed and normalized by mloess method[45]. Genes differentially regulated between WT and *Rel*$^{-/-}$*Relb*$^{-/-}$ BMDCs during TLR stimulation time courses were analyzed by two-class paired SAM[46] implemented in the MeV program (multiple expression viewer)[47]. Class pairing was defined by corresponding time points between WT and *Rel*$^{-/-}$*Relb*$^{-/-}$ BMDCs. Differentially expressed genes identified at the false discovery rate below 5% were deemed significant. Genes with at least twofold induction during TLR-elicited DC maturation are listed in **Supplementary Table 1**. In heat maps, expression values of each gene were normalized to its maximum fold induction and clustered by hierarchical clustering with Euclidian distance (**Fig. 5e**). For phenotyping analyses (**Fig. 5f** and **Supplementary Table 2**), the average fold induction (FI)[26] in $\log_2$ scale across either timecourse (CpG and Pam_3CSK_4) was calculated for different genotypes, for example, FI_{WT}, $FI_{Rel-/-}$, and $FI_{Rel-/-Relb-/-}$. The RelB phenotype was defined as $FI_{WT}-FI_{Rel-/-}$, the c-Rel-RelB phenotype was defined as $FI_{WT}-FI_{Rel-/-Relb-/-}$. Quantitative (q)RT-PCR was performed after first-strand cDNA synthesis with oligo(dT) and SuperScript RT II (Invitrogen), using SYBR Green PCR Master Mix reagent (Stratagene), Eppendorf Mastercycler realplex system and gene-specific primers (**Supplementary Table 3**). Data analysis used the Δ(ΔCt) method with β-actin as normalization control to relate signals to those in MEFs or derive fold induction over basal levels. qRT-PCR and chromatin immunoprecipitation data shown are representative of three independent experiments (mean ± s.d.). Quantification of mRNA and protein abundance are representative of four independent experiments.

Computational modeling. The RelA–RelB mathematical model (version 5.0) involving mass action kinetic equations was developed based on a previously published model (version 3.1)[22] and experimental data[20] that allowed for constraints-based parameterization. Refinement of the model (version 5.1) and MEF- and DC-specific parameterization were based on experimental data presented in this paper. Computational simulations were performed in Matlab using the ode15s solver. Detailed descriptions are included in the **Supplementary Note**.

Statistics. Statistical significance was calculated by two-tailed Student's *t*-test with Prism software (GraphPad). Error bars were shown as either s.d. or s.e.m. as indicated.

42. Lutz, M.B. *et al.* An advanced culture method for generating large quantities of highly pure dendritic cells from mouse bone marrow. *J. Immunol. Methods* **223**, 77–92 (1999).
43. Boonstra, A. *et al.* Flexibility of mouse classical and plasmacytoid-derived dendritic cells in directing T helper type 1 and 2 cell development: dependency on antigen dose and differential toll-like receptor ligation. *J. Exp. Med.* **197**, 101–109 (2003).

44. Cheng, C.S. *et al.* The specificity of innate immune responses is enforced by repression of interferon response elements by NF-κB p50. *Sci. Signal.* **4**, ra11 (2011).
45. Sasik, R., Woelk, C.H. & Corbeil, J. Microarray truths and consequences. *J. Mol. Endocrinol.* **33**, 1–9 (2004).
46. Tusher, V.G., Tibshirani, R. & Chu, G. Significance analysis of microarrays applied to the ionizing radiation response. *Proc. Natl. Acad. Sci. USA* **98**, 5116–5121 (2001).
47. Saeed, A.I. *et al.* TM4 microarray software suite. *Methods Enzymol.* **411**, 134–193 (2006).

doi:10.1038/ni.2446

nature COMMUNICATIONS

OPEN

ARTICLE

Received 17 Apr 2012 | Accepted 18 Jun 2012 | Published 17 Jul 2012

DOI: 10.1038/ncomms1960

Epidermal phospholipase Cδ1 regulates granulocyte counts and systemic interleukin-17 levels in mice

Kaori Kanemaru[1,*], Yoshikazu Nakamura[1,*], Kojiro Sato[2], Ryota Kojima[1], Saori Takahashi[1], Mami Yamaguchi[1], Manabu Ichinohe[1], Hiroshi Kiyonari[3], Go Shioi[3], Kenji Kabashima[4], Kyoko Nakahigashi[4], Masataka Asagiri[5,6], Colin Jamora[7], Hideki Yamaguchi[8] & Kiyoko Fukami[1]

Phospholipase C is a key enzyme in phosphoinositide turnover. Although its functions have been extensively studied at the cellular level, many questions remain concerning its functions at the organ and individual animal levels. Here we demonstrate that mice lacking *phospholipase Cδ1* develop granulocytosis associated with elevated serum levels of the granulopoietic cytokine interleukin-17. Re-introduction of *phospholipase Cδ1* into keratinocytes of *phospholipase Cδ1*-deficient mice reverses this phenotype, whereas conditional ablation of *phospholipase Cδ1* in keratinocytes recreates it. Interleukin-17 and its key upstream regulator interleukin-23 are also upregulated in epidermis. Loss of *phospholipase Cδ1* from keratinocytes causes features of interleukin-17-associated inflammatory skin diseases. Phospholipase Cδ1 protein is downregulated in the epidermis of human psoriatic skin and in a mouse model of psoriasis. These results demonstrate that phosphoinositide turnover in keratinocytes regulates not only local inflammatory responses but also serum cytokine levels and systemic leukocyte counts, and affects distant haematopoietic organs.

[1] Laboratory of Genome and Biosignal, Tokyo University of Pharmacy and Life Sciences, Hachioji-shi, Tokyo 192-0392, Japan. [2] Department of Rheumatology and Applied Immunology, Faculty of Medicine, Saitama Medical University, Iruma-gun, Saitama 350-0495, Japan. [3] Laboratory for Animal Resources and Genetic Engineering, RIKEN Center for Developmental Biology, Kobe-shi, Hyogo 650-0047, Japan. [4] Department of Dermatology, Graduate School of Medicine, Kyoto University, Sakyo-ku, Kyoto 606-8507, Japan. [5] Department of Chemistry and Biochemistry, University of California San Diego, La Jolla, California 92093, USA. [6] Innovation Center for Immunoregulation and Therapeutics, Graduate School of Medicine, Kyoto University, Sakyo-ku, Kyoto 606-8501, Japan. [7] Section of Cell and Developmental Biology, Division of Biological Sciences, University of California San Diego, La Jolla, California 92093, USA. [8] Division of Metastasis and Invasion Signaling, National Cancer Center Research Institute, Chuo-ku, Tokyo 104-0045, Japan. *These authors contributed equally to this work. Correspondence and requests for materials should be addressed to Y.N. (email: ynakamur@toyaku.ac.jp) or to K.F. (email: kfukami@toyaku.ac.jp).

Phospholipase C (PLC) is a key enzyme in phosphoinositide turnover, an important signal transduction process in cells. PLC hydrolyses phosphatidylinositol 4,5-bisphosphate (PIP_2) to generate the second messengers inositol 1,4,5-trisphosphate (IP_3) and diacylglycerol (DAG), leading to elevated intracellular calcium ion concentrations and activation of protein kinase C (PKC)[1,2]. Although the functions of PLC have been extensively studied at the single-cell level[3], its physiological role in interactions among different cell types *in vivo* remains largely unknown.

Humoural factors communicate between different, distantly located cell types, and induce various physiological and cellular events such as inflammation, cell growth and apoptosis. Cytokines are one type of such humoural factors. Interleukin (IL)-17, also called IL-17A, is a pleiotropic cytokine that has emerged as a central player in the mammalian immune system, with important roles in the pathology of many disease processes, including allergic responses[4] and autoimmune diseases[5–10]. IL-17 is mainly produced by T lymphocytes under the regulation of IL-23 (refs 11,12), and in turn, regulates granulopoiesis through induction of granulocyte colony-stimulating factor (G-CSF)[13–15]. Granulocytes are key players in the pathogenesis of several inflammatory diseases. Increased baseline circulating granulocyte number is a risk factor for all-cause mortality and the progression of chronic diseases such as atherosclerosis and chronic renal failure[16–18].

We previously reported that one of the PLC isozymes, PLCδ1, was abundantly expressed in the epidermis[19] and that systemic loss of PLCδ1 resulted in epidermal hyperplasia associated with the infiltration of immune cells[20]. The epidermis is mainly composed of keratinocytes and is characterized by a polarized pattern of epithelial growth and differentiation, with a single basal layer of proliferating keratinocytes and multiple, overlying differentiated layers. Epidermal keratinocytes not only act as a barrier to the external environment, but also exert important functions in skin immune responses by secreting a variety of cytokines that initiate local inflammatory responses[21]. Indeed, keratinocytes have pivotal roles in the pathogenesis of human inflammatory skin diseases, including psoriasis and atopic dermatitis[22]. However, little is known about the ability of keratinocytes to regulate systemic inflammatory responses.

Here we demonstrate that loss of epidermal PLCδ1 results not only in skin inflammation associated with aberrant activation of IL-23/IL-17 axis, but also in systemic inflammation, characterized by increase in serum cytokine levels and systemic granulocytosis.

Results

Loss of systemic PLCδ1 causes granulocytosis. Loss of PLCβ3 in haematopoietic cells alters blood cell counts and populations in a haematopoietic cell intrinsic manner[23]. As PLCβ3 binds to PLCδ1 (ref. 24) in a manner similar to the binding of PLCβ2, we investigated if the systemic loss of PLCδ1 also affected blood cell counts and populations. Mice lacking the *PLCδ1* gene (*PLCδ1*$^{-/-}$ mice) exhibited a greater than twofold increase in peripheral blood leukocytes compared with wild-type mice (mean±s.e.m. cell numbers, $9.2\pm0.85\times10^6$ in wild-type versus $19\pm1.4\times10^6$ in *PLCδ1*$^{-/-}$ mice, $n=6$ for wild-type and $n=9$ for *PLCδ1*$^{-/-}$ mice). We also examined the population of CD11b$^+$ Gr-1$^+$ granulocytes. At first, we confirmed that *PLCδ1*$^{+/-}$ mice did not exhibit increase in granulocytes (Supplementary Fig. S1), and *PLCδ1*$^{+/-}$ mice were, therefore, used as a control in subsequent experiments. Granulocytes were markedly increased in the peripheral blood leukocyte in *PLCδ1*$^{-/-}$ mice, as well as in the spleen and bone marrow (Fig. 1a;

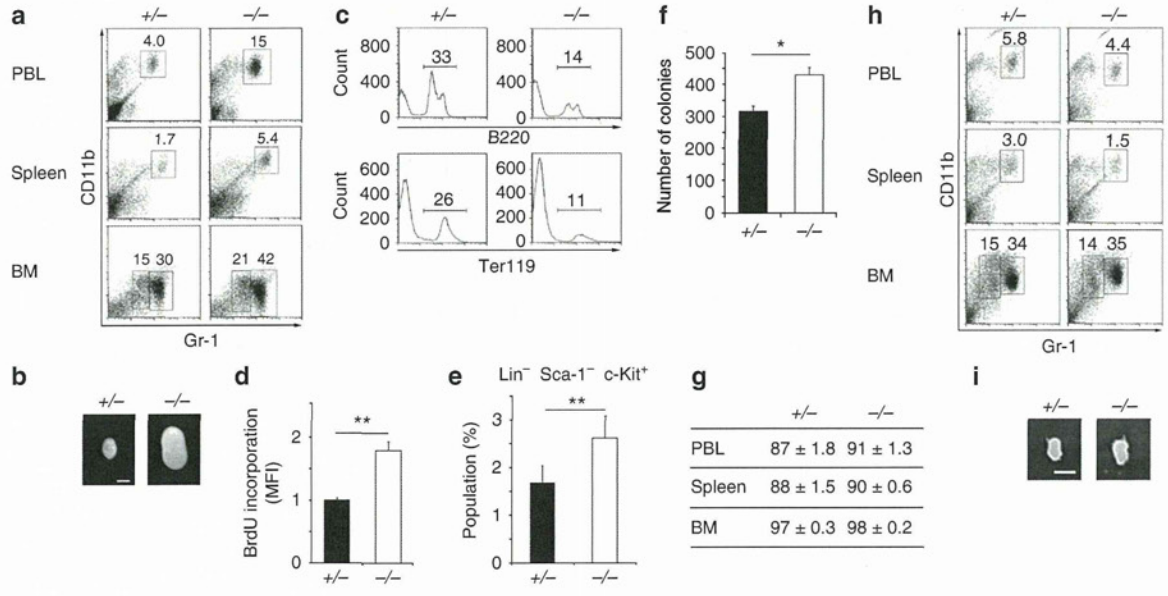

Figure 1 | *PLCδ1*$^{-/-}$ mice show granulocytosis in non-haematopoietic cell intrinsic manner. (**a**) Representative FACS profiles of CD11b$^+$ Gr-1$^+$ granulocytes in peripheral blood leukocytes (PBL), spleen, and bone marrow (BM) ($n=14$). Granulocytes in bone marrow were categorized into immature (CD11b$^+$ Gr-1^{low}) and mature (CD11b$^+$ Gr-1^{high}) subsets. (**b**) Macroscopic appearance of ILNs. Scale bar, 2 mm. (**c**) Representative FACS profiles of B220$^+$ and Ter119$^+$ cells in the BM ($n=7$–12). (**d**) BrdU incorporation in immature granulocytes (CD11b$^+$ Gr-1^{low}) in the BM. Data are expressed as the relative mean fluorescence intensity (MFI)±s.e.m. (MFI of *PLCδ1*$^{+/-}$ mice = 1) ($n=5$). (**e**) Populations of myeloid progenitor-rich Lin$^-$ Sca-1$^-$ c-Kit$^+$ cells in the BM. Mean±s.e.m. ($n=8$). (**f**) *In vitro* colony-forming assay. The numbers of colony-forming cells per 6×10^4 cells at 12 days after plating are displayed. Mean±s.e.m. ($n=4$). (**g**) Haematopoietic chimerism analysis. Chimerism of the PBL, spleen, and BM were determined in transplanted mice by FACS analysis of CD45.1$^-$ cells. Mean percentage±s.e.m. Six recipients in each group. Three donor mice per genotype were used. (**h**) Representative FACS profiles of CD45.1$^-$ CD11b$^+$ Gr-1$^+$ granulocytes in the PBL, spleen, and BM of CD45.1$^+$ congenic recipients reconstituted with *PLCδ1*$^{+/-}$ or *PLCδ1*$^{-/-}$ BM at 4 weeks post-transplantation. ($n=6$). Plots shown are gated on CD45.1$^-$ cells. (**i**) Macroscopic appearance of the ILNs. Scale bar, 2 mm. Mice used in all experiments were 8–12 weeks old. Statistical significance was assessed using a Student's *t*-test. *$P<0.05$; **$P<0.01$.

Table 1 | Absolute numbers of granulocytes, erythrocytes, and B and T lymphocytes in peripheral blood, spleen, bone marrow, and inguinal lymph nodes.

	Gr-1$^+$ CD11b$^+$	B220$^+$	Ter119$^+$	CD3$^+$
PBL				
PLCδ1$^{+/-}$	6.7±0.5 (*n*=6)	NA	NA	NA
PLCδ1$^{-/-}$	20.3±2.1** (*n*=9)	NA	NA	NA
Spleen				
PLCδ1$^{+/-}$	23±5.5 (*n*=10)	NA	NA	NA
PLCδ1$^{-/-}$	57±9.3** (*n*=10)	NA	NA	NA
BM				
PLCδ1$^{+/-}$	204±29 (*n*=12)	85±9.4 (*n*=12)	75±18 (*n*=7)	NA
PLCδ1$^{-/-}$	248±41* (*n*=12)	50±5.7* (*n*=12)	45±7.3* (*n*=7)	NA
ILNs				
PLCδ1$^{+/-}$	3.2±0.4 (*n*=5)	9.4±1.9 (*n*=4)	NA	40±1.0 (*n*=7)
PLCδ1$^{-/-}$	11.2±0.9** (*n*=5)	31.6±5.2** (*n*=4)	NA	81±1.6** (*n*=7)

NA, not available; PBL, peripheral blood lymphocytes; BM, bone marrow; INLs, inguinal lymph nodes.
Cell numbers are represented as number×10^5±s.e.m.
For ILNs, Gr-1$^+$ cells were counted, instead of Gr-1$^+$ CD11b$^+$ cells.
Statistical significance was assessed using a Student's *t*-test.
*P<0.05.
**P<0.01.

Table 1). *PLCδ1*$^{-/-}$ mice also showed lymphadenopathy of the inguinal lymph nodes (ILNs) and mild splenomegaly (Fig. 1b; Supplementary Table S1). We confirmed that expression of other PLC isoforms was not affected by loss of PLCδ1 (Supplementary Fig. S2). Antibiotic treatment of *PLCδ1*$^{-/-}$ mice had no effect on the development of granulocytosis and lymphadenopathy (Supplementary Fig. S3a–d), and *PLCδ1*$^{-/-}$ granulocytes seemed to be morphologically and functionally normal (Supplementary Fig. S4a–c), suggesting that the observed granulocytosis was not a secondary effect of bacterial infection or impaired granulocyte function. Enhanced granulopoiesis in the bone marrow is often accompanied by a reduction of B lymphocytes and erythrocytes[25–27], and reduced numbers of B220$^+$ B lymphocytes and Ter119$^+$ erythrocytes were indeed observed in the bone marrow of *PLCδ1*$^{-/-}$ mice (Fig. 1c; Table 1). Granulocytes in mouse bone marrow can be categorized into immature and mature subsets[28], both of which were elevated in *PLCδ1*$^{-/-}$ bone marrow (Fig. 1a), suggesting that the increase in the granulocyte population arose from an immature progenitor population. A 5-bromo-2′-deoxy-uridine (BrdU) incorporation assay revealed that the proliferative activity of immature granulocytes was higher in *PLCδ1*$^{-/-}$ than in *PLCδ1*$^{+/-}$ bone marrow (Fig. 1d), suggesting that the increase in granulocyte number resulted from enhanced proliferation of immature granulocytes. An increased population of myeloid progenitor cells could also increase the granulocyte number in *PLCδ1*$^{-/-}$ mice. Indeed, the population of myeloid progenitor cells was greater in the bone marrow of *PLCδ1*$^{-/-}$ than of *PLCδ1*$^{+/-}$ mice (Fig. 1e), as was the number of myeloid colony-forming units (Fig. 1f), indicating that the loss of *PLCδ1* resulted in an increased population of myeloid progenitor cells in the bone marrow, possibly leading to granulocytosis.

As granulocytosis in *PLCδ1*$^{-/-}$ mice was likely caused by the lack of *PLCδ1* in the haematopoietic compartment, we generated mice lacking *PLCδ1* in the haematopoietic compartment by bone marrow transfer. Surprisingly, mice transplanted with *PLCδ1*$^{-/-}$ bone marrow did not develop granulocytosis or lymphadenopathy (Fig. 1g–i), indicating that the loss of *PLCδ1* in the haematopoietic system was not responsible for these phenotypes, and that the mechanism of granulocytosis in *PLCδ1*$^{-/-}$ mice differed from that in mice lacking PLCβ3 (ref. 23).

***PLCδ1*$^{-/-}$ mice display local and systemic IL-17 upregulation.** The granulocyte population was increased and the B220$^+$ B lymphocyte and Ter119$^+$ erythrocyte populations were decreased in the bone marrow of *PLCδ1*$^{-/-}$ mice (Fig. 1a,c; Table 1). However, the balance among colony-forming unit (CFU)- granulocyte/erythroid/macrophage/megakaryocyte, -granulocyte/macrophage, -macrophage, -granulocyte, and burst-forming unit-erythroid (BFU-E) was not dramatically disrupted in *PLCδ1*$^{-/-}$ bone marrow cells cultured *in vitro* (Supplementary Fig. S5). We therefore speculated that granulocytosis in *PLCδ1*$^{-/-}$ mice was induced by humoural factors secreted from peripheral tissues. IL-17 is a critical cytokine for granulopoiesis[13–15], and we, therefore, assessed serum IL-17 concentrations. IL-17 levels in the serum of control mice were below the detection limit, but those in *PLCδ1*$^{-/-}$ mice were detectable (Fig. 2a), indicating that circulating levels of the granulopoietic cytokine IL-17 were increased in *PLCδ1*$^{-/-}$ mice. The concentrations of other granulopoietic factors were not increased in *PLCδ1*$^{-/-}$ mice (Supplementary Fig. S6), strongly suggesting that IL-17 elevation is responsible for granulocytosis in these mice.

We investigated IL-17 production by lymphocytes in lymph nodes including ILNs and mesenteric lymph nodes (MLNs) by intracellular cytokine staining. The population of IL-17-producing cells was increased in ILNs, but not in MLNs, in *PLCδ1*$^{-/-}$ mice (Fig. 2b). The number of IL-17-producing cells in the ILNs of *PLCδ1*$^{-/-}$ mice exhibited a 3.9-fold increase compared with that in *PLCδ1*$^{+/-}$ mice (Fig. 2c). *IL-17* messenger RNA expression in ILNs, analysed using real-time RT–PCR was increased in *PLCδ1*$^{-/-}$ mice (Fig. 2d). We then investigated the specific cellular source of IL-17 in ILNs of *PLCδ1*$^{-/-}$ mice. Fluorescence-activated cell sorting (FACS) analysis revealed that the main producers of IL-17 were the γδ-T-cell receptor (TCR)-positive T cells (Fig. 2e). ILNs are skin-draining, whereas MLNs are not, suggesting that IL-17 was specifically upregulated in skin-draining lymph nodes. Indeed, another type of skin-draining lymph nodes, the axillary lymph nodes, also expressed high levels of *IL-17* mRNA (Fig. 2f). These results suggest that the skin system has a pivotal role in IL-17 upregulation. Importantly, *IL-17* expression was detected in *PLCδ1*$^{-/-}$ skin, but not in normal skin (Fig. 2g). In contrast to IL-17, the expression of *interferon γ* and *IL-4* was not increased in skin of *PLCδ1*$^{-/-}$ mice (Supplementary Fig. S7a). Thus, *PLCδ1*$^{-/-}$ mice showed IL-17 upregulation in skin and skin-draining lymph nodes.

Epidermal PLCδ1 is sufficient for normal IL-17 levels. Among skin cells, keratinocytes express the highest levels of PLCδ1 (ref. 19). In addition, IL-17 was upregulated in skin and skin-draining lymph nodes. We, therefore, hypothesized that the PLCδ1 in keratinocytes primarily regulates IL-17 levels. To test this hypothesis, we investigated whether reintroduction of *PLCδ1* into keratinocytes of *PLCδ1*$^{-/-}$ mice could restore normal IL-17 levels. We previously reported that expression of PLCδ1 in keratinocytes was mainly regulated by the transcription factor Foxn1 (ref. 29) and we, therefore, used a *Foxn1* promoter-driven *PLCδ1* gene (*Foxn1::PLCδ1*) (Fig. 3a) to restore PLCδ1 expression in *PLCδ1*$^{-/-}$ keratinocytes in a manner resembling that of endogenous *PLCδ1*. Mice carrying *Foxn1::PLCδ1* (Fig. 3b) appeared normal and did not exhibit any overt changes. Intercrossing *PLCδ1*$^{-/-}$ mice and mice carrying *Foxn1::*

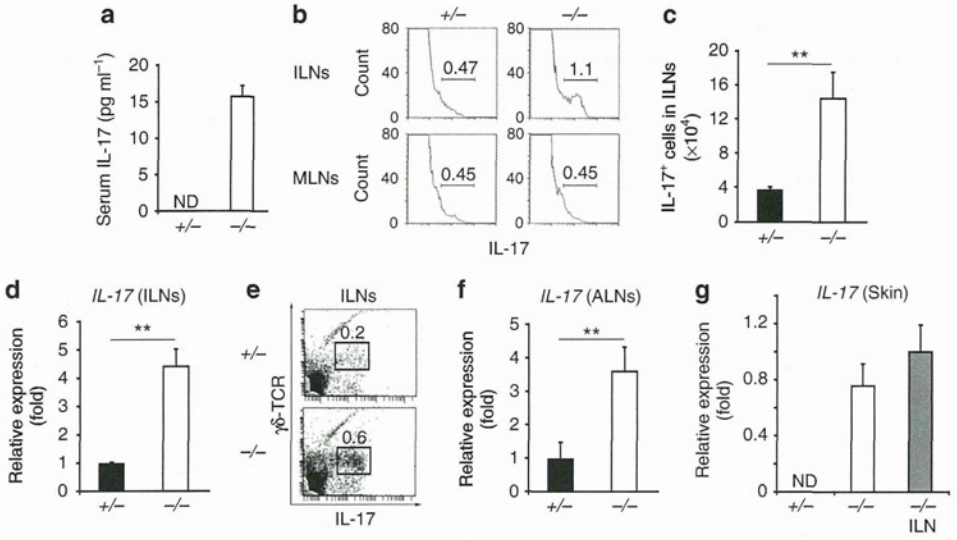

Figure 2 | Local and systemic IL-17 upregulation in *PLCδ1*$^{-/-}$ mice. (**a**) IL-17 concentration in the serum measured by ELISA. Mean±s.e.m. ($n=6$). (**b**) Representative FACS profiles of intracellular IL-17 in ILNs and MLNs. Cells were stimulated and intracellular IL-17 was detected ($n=6$ for ILNs and $n=3$ for MLNs). Three independent experiments were performed. (**c**) Absolute numbers of IL-17$^+$ cells in ILNs. Mean±s.e.m. ($n=6$). The combined results from three independent experiments are displayed. (**d**) *IL-17* mRNA expression in the ILNs determined by real-time RT-PCR. All values are normalized to *glyceraldehyde 3-phosphate dehydrogenase* (*GAPDH*). Results are displayed as arbitrary units (expression in *PLCδ1*$^{+/-}$ mice=1). Mean±s.e.m. ($n=3$). (**e**) Representative FACS profiles of γδ-TCR and intracellular IL-17 in ILNs ($n=3$). Cells were stimulated and intracellular IL-17 was detected. Three independent experiments were performed. (**f**) *IL-17* mRNA expression in the axillary lymph nodes (ALNs) determined by real-time RT-PCR. All values are normalized to *GAPDH*. Results are displayed as arbitrary units (expression in *PLCδ1*$^{+/-}$ mice=1). Mean±s.e.m. ($n=5$). (**g**) *IL-17* mRNA expression in skin determined by real-time RT-PCR. *PLCδ1*$^{-/-}$ ILN was used as the positive control for *IL-17* expression. All values are normalized to *GAPDH*. Results are displayed as arbitrary units (expression in *PLCδ1*$^{-/-}$ ILN=1). Mean±s.e.m. ($n=5$). Mice used in all experiments were 8–12 weeks old. Statistical significance was assessed using a Student's *t*-test. $^{**}P<0.01$. ND; not detected.

PLCδ1 produced *PLCδ1*$^{-/-}$ mice carrying *Foxn1::PLCδ1* (*Tg/KO* mice). PLCδ1 expression was restored in the skin of *Tg/KO* mice, but not in other organs such as the lungs, brain, ILNs, spleen and bone marrow (Fig. 3c). PLCδ1 protein was weakly expressed in *Tg/KO* thymuses, but these thymuses did not show obvious phenotypes, such as a disturbed balance of T-cell subtypes. Although the level of expression of PLCδ1 protein was somewhat lower in *Tg/KO* than in wild-type and heterozygous skin (Supplementary Fig. S8), the immunofluorescence observation indicated that both endogenous and transgene-derived PLCδ1 protein was expressed in suprabasal epidermis (Fig. 3d). These expression patterns were consistent with enriched expression of PLCδ1 and Foxn1 in differentiated keratinocytes[29,30]. At the histological level, the introduction of *Foxn1::PLCδ1* gene rescued epidermal hyperplasia and immune cell infiltration that were observed in *PLCδ1*$^{-/-}$ mice[20] (Fig. 3e,f). Importantly, *IL-17* expression was remarkably decreased in *Tg/KO* skin (Fig. 3g) compared with *PLCδ1*$^{-/-}$ skin. Residual expression of *IL-17* mRNA in *Tg/KO* skin may be caused by a lower level of PLCδ1 protein expression in *Tg/KO* than in control skin. *Tg/KO* mice showed no lymphadenopathy of the ILNs (Fig. 3h, Supplementary Table S2), and IL-17-producing cells were not increased in the ILNs in *Tg/KO* mice (Fig. 3i,j). Thus, reintroduction of *PLCδ1* into keratinocytes ameliorated local IL-17 upregulation. In addition, IL-17 concentrations in the serum of *Tg/KO* mice reverted to undetectable levels as in control mice (Fig. 3k), strongly suggesting that skin- and skin-draining lymph node-derived IL-17 was required for the elevation of IL-17 levels in serum. We also examined granulocyte populations in the peripheral blood, spleen, and bone marrow. Interestingly, *Tg/KO* mice did not exhibit granulocytosis (Fig. 3l), suggesting a close correlation between granulocytosis and IL-17 levels. These observations indicate that PLCδ1 expression in keratinocytes was sufficient for normal granulocyte counts and IL-17 levels in *PLCδ1*$^{-/-}$ mice.

Epidermal PLCδ1 regulates local and systemic IL-17 levels. We examined whether loss of PLCδ1 in keratinocytes caused IL-17 upregulation and granulocytosis by generating keratinocyte-specific conditional *PLCδ1*-knockout (*cKO*) mice with *K14* promoter-driven *Cre* transgenic mice (Fig. 4a,b). We confirmed that PLCδ1 was deleted in the epidermis of the *cKO* mice and that its expression was not altered in other organs such as the lungs, brain, ILNs, spleen, and bone marrow (Fig. 4c). As the *K14* promoter is active in the thymus, we examined the expression of PLCδ1 in the thymus, finding that PLCδ1 was downregulated in the thymus of *cKO* mice (Fig. 4c). However, we did not observe any obvious abnormalities in *cKO* thymus. *IL-17* was upregulated in the skin of *cKO* mice (Fig. 4d), whereas *interferon γ* and *IL-4* expression levels remained unchanged (Supplementary Fig. S7b). Interestingly, *IL-17* mRNA was upregulated more in the epidermis than in whole skin of *cKO* mice (Fig. 4e). CD3-positive T cells were major IL-17 producers in the *cKO* epidermis (Fig. 4f). The number of CD3-positive T cells was 1.7-fold higher in *cKO* than in control epidermis, suggesting that upregulation of *IL-17* mRNA in *cKO* epidermis is due, at least in part, to an increase in T cells. Further analysis revealed that *IL-17* was expressed by Vγ3-positive γδ T cells in *cKO* epidermis (Supplementary Fig. S9a). We also found that the level of *IL-17* mRNA was not significantly altered by depletion of Langerhans cells (Supplementary Fig. S9b). *cKO* mice also showed increased ILN size (Fig. 4g; Supplementary Table S3) and cell numbers (mean±s.e.m. cell numbers, $3.7\pm0.9\times10^6$ in controls versus $14\pm2.4\times10^6$ in *cKO* mice, both $n=6$). The number of IL-17-producing cells in the ILNs of *cKO* mice was more than six times that in the control mice (Fig. 4h).

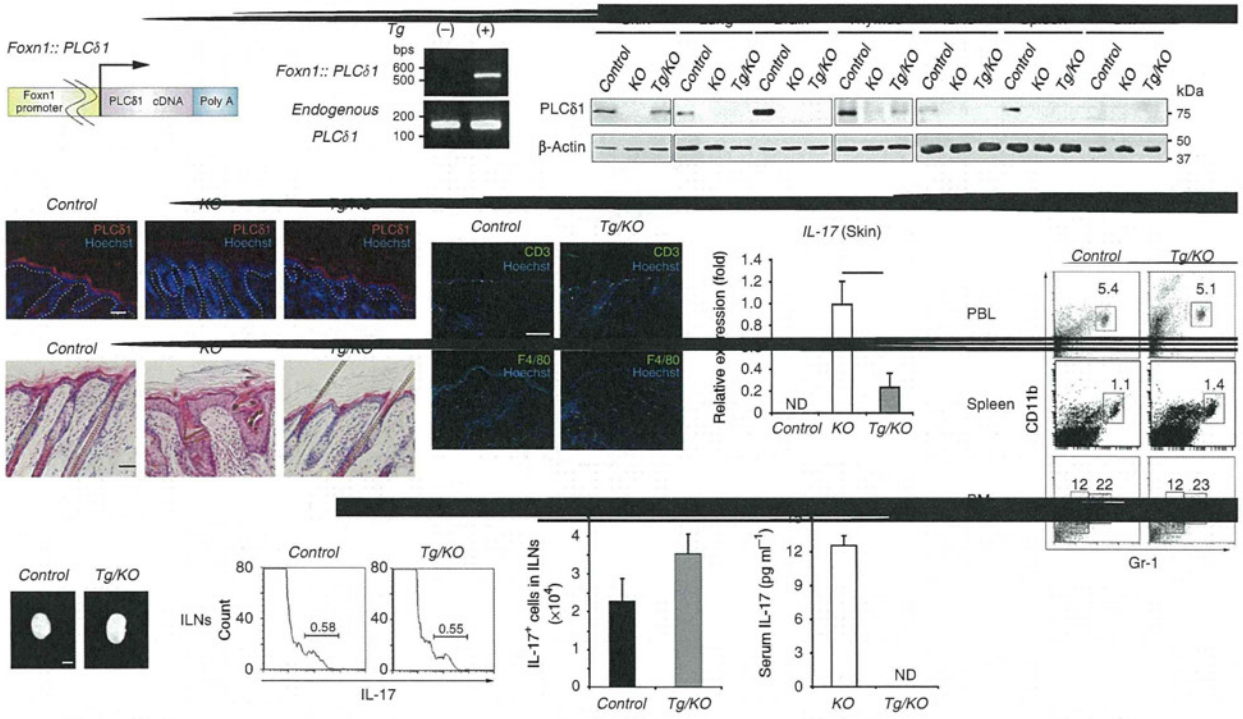

Figure 3 | Reintroduction of PLCδ1 in *PLCδ1*$^{-/-}$ keratinocytes restores normal IL-17 levels and granulocyte counts. (**a**) Structure of the *Foxn1::PLCδ1* gene. Poly A: the bovine growth hormone polyadenylation sequence. (**b**) PCR analysis of genomic DNA from the tails of *wild-type* and *Foxn1::PLCδ1* Tg mice. Products derived from *Foxn1::PLCδ1* and endogenous *PLCδ1*. (**c**) Immunoblotting of PLCδ1 and β-actin in tissues from control, *PLCδ1*$^{-/-}$ (*KO*), and *Tg/KO* mice. (**d**) Skin stained with antibody against PLCδ1 (red) and Hoechst stain (blue). Dotted lines denote the dermal-epidermal border. Scale bar, 50 μm. (**e**) Haematoxylin-eosin (HE) stained dorsal skin sections. Scale bar, 50 μm. (**f**) The skin was stained with antibodies against CD3 (green) or F4/80 (green) and Hoechst (blue). Scale bar, 100 μm. (**g**) *IL-17* mRNA expression in the skin of control, *PLCδ1*$^{-/-}$ (*KO*), and *Tg/KO* mice determined by real-time RT-PCR. All values are normalized to *GAPDH*. Results are displayed as arbitrary units (expression in the skin of *KO* mice = 1). Mean±s.e.m. ($n=5$). (**h**) Macroscopic appearance of ILNs in control and *Tg/KO* mice. Scale bar, 1 mm. (**i**) Representative FACS profiles of intracellular IL-17 in ILNs. Cells were stimulated and intracellular IL-17 was detected ($n=4$). Three independent experiments were performed. (**j**) Absolute numbers of IL-17$^+$ cells. Mean±s.e.m. ($n=4$). The combined results from three independent experiments are displayed. (**k**) IL-17 concentration in serum measured by ELISA. Mean±s.e.m. ($n=3$). (**l**) Representative FACS profiles of CD11b$^+$ Gr-1$^+$ granulocytes in the PBL, spleen, and BM of *Tg/KO* mice ($n=4$). (**d**–**l**) 8–12-week-old mice were used. (**d**–**j**, **l**) Heterozygotes with *Foxn1::PLCδ1* were used as controls. Statistical significance was assessed using a Student's *t*-test. $^{**}P<0.01$. ND, not detected.

The main IL-17-producing cells in *cKO* ILNs were γδ T cells (Fig. 4i). *IL-17* upregulation in ILNs of *cKO* mice was also confirmed by real-time RT–PCR (Fig. 4j). Production of the granulopoietic cytokine G-CSF is induced by IL-17 in many cell types, and we, therefore, examined whether conditioned medium (CM) derived from cKO skin-draining lymph nodes induced *G-CSF* expression. CM from *cKO* skin-draining lymph nodes induced higher *G-CSF* expression in fibroblasts compared with CM from control skin-draining lymph nodes (Fig. 4k). Importantly, CM from *cKO* skin-draining lymph nodes pretreated with anti-IL-17 neutralizing antibody did not cause *G-CSF* upregulation (Fig. 4k), strongly suggesting that cells in the *cKO* skin-draining lymph nodes secrete IL-17, leading to *G-CSF* production. If IL-17 derived from skin and skin-draining lymph nodes causes serum IL-17 elevation, then serum IL-17 concentrations should also be increased in *cKO* mice. Indeed, serum IL-17 levels were high in *cKO* mice (Fig. 4l), strongly suggesting that local IL-17 upregulation is linked to elevation of serum IL-17 levels. In addition, serum G-CSF concentrations were significantly increased in *cKO* mice compared with control mice (Fig. 4m). We further investigated the granulocyte population in *cKO* mice and found that *cKO* mice showed granulocytosis (Fig. 4n), consistent with local and serum IL-17 upregulation. Reduced numbers of bone marrow B lymphocytes and erythrocytes were also observed in *cKO* mice (Supplementary Fig. S10). Taken together, these results indicate that PLCδ1 in keratinocytes is required for the maintenance of normal IL-17 levels and granulocyte counts.

Epidermal PLCδ1 regulates IL-23 expression in the skin. We investigated the mechanisms of IL-17 upregulation in the epidermis by analysing the expression of the IL-17-inducing cytokine, IL-23. IL-23 and IL-12 are functionally related as heterodimeric cytokines that share the IL-12/23p40 subunit[31]. The mRNAs for the subunits of the IL-23 heterodimer (*IL-12/23p40* and *IL-23p19*) were upregulated in *cKO* skin (Fig. 5a), while *IL-12p35*, which encodes the IL-12-specific subunit, was not upregulated (Fig. 5a). In contrast, a dramatic decrease in *IL-23* expression was detected after reintroduction of PLCδ1 into keratinocytes (Supplementary Fig. S11). As *Tg/KO* skin showed no drastic increase in *IL-17* (Fig. 3g) whereas *cKO* skin showed remarkable *IL-17* upregulation (Fig. 4d), the expression level of *IL-23* was closely correlated with that of *IL-17* in skin. Similar to IL-17, IL-23p19 mRNA and protein were upregulated in cKO epidermis (Fig. 5b,c). Immunofluorescence experiments showed faint IL-23p19 immunoreactivity in control epidermis, whereas keratinocytes in the basal layer of *cKO* epidermis showed strong IL-23p19 immunoreactivity (Fig. 5d). *IL-23p19* expression was also assessed in primary keratinocyte cultures. *cKO* keratinocytes did not show

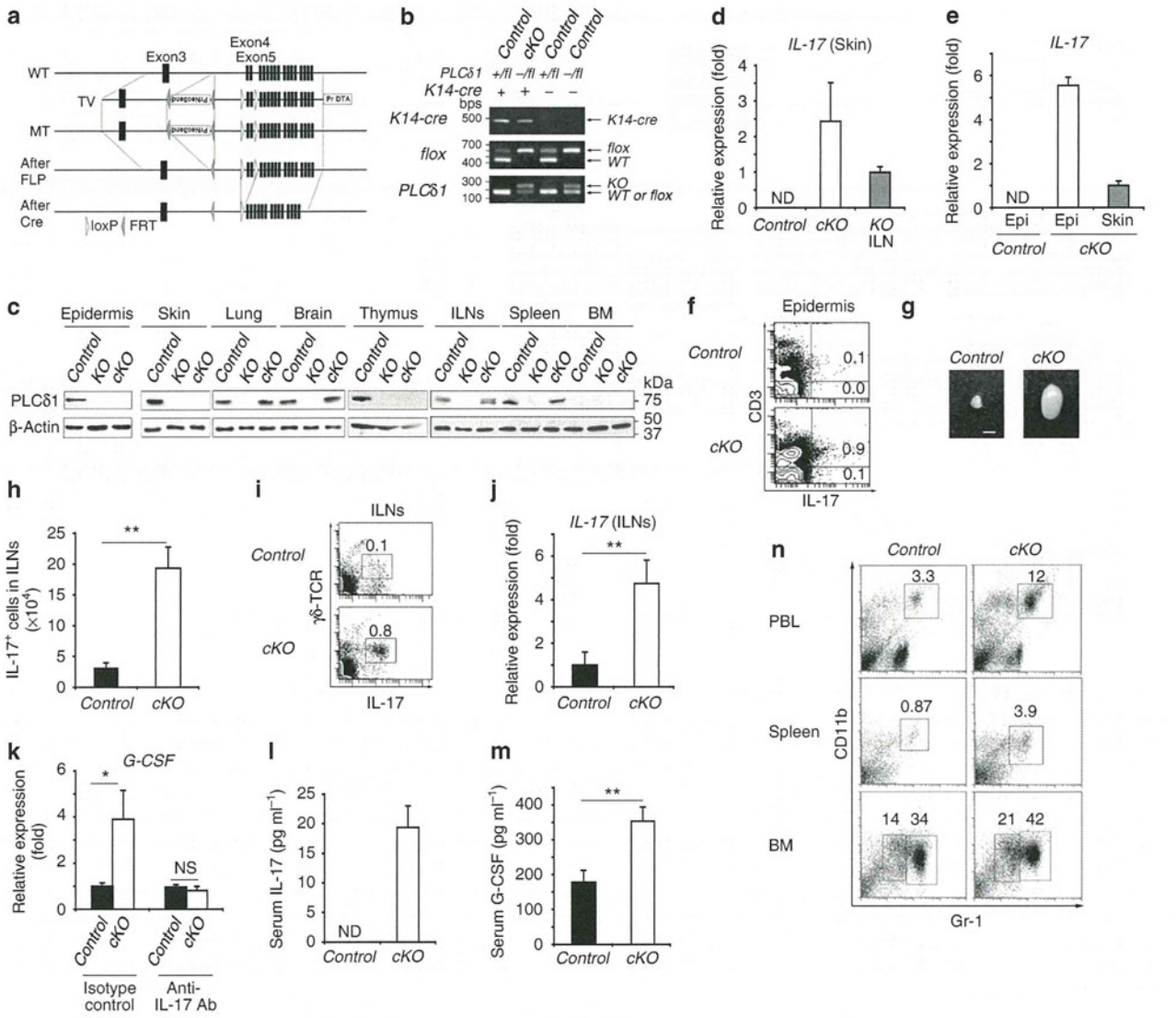

Figure 4 | Epidermal loss of PLCδ1 results in IL-17 upregulation and granulocytosis. (**a**) Genomic structure of the *PLCδ1* gene (WT). Exons are indicated by filled boxes. The structures of the targeting vector (TV) for disrupting the mouse *PLCδ1*, targeted allele (MT), allele after FLP recombination (After FLP), and allele after Cre recombination (After Cre) are displayed. (**b**) PCR genotyping of control and *cKO* mice. (**c**) Immunoblotting of PLCδ1 and β-actin in tissues from control, *PLCδ1*$^{-/-}$ (*KO*), and *cKO* mice. (**d**) *IL-17* mRNA expression in skin. *KO* ILN was used as positive control for *IL-17* expression. Results are displayed as arbitrary units (expression in *KO* ILN = 1). Mean ± s.e.m. ($n = 3$). (**e**) *IL-17* mRNA expression in epidermis (epi) and whole skin (skin). Results are displayed as arbitrary units (expression in *cKO* whole skin = 1). Mean ± s.e.m. ($n = 3$). (**f**) Representative FACS profiles of IL-17 and CD3 of epidermis ($n = 3$). Three independent experiments were performed. (**g**) Macroscopic appearance of ILNs. Scale bar = 2 mm. (**h**) Absolute numbers of IL-17$^+$ cells in ILNs. Mean ± s.e.m. ($n = 6$). (**i**) Representative FACS profiles of γδ-TCR and intracellular IL-17 in ILNs ($n = 6$). Cells were stimulated. Five independent experiments were performed. (**j**) *IL-17* mRNA expression in the ILNs. Results are listed as arbitrary units (expression in control mice = 1). Mean ± s.e.m. ($n = 3$). (**k**) *G-CSF* expression in Swiss 3T3 cells treated with skin-draining lymph-node CM in the presence of anti-IL-17 neutralizing antibody or isotype control. Results are displayed as arbitrary units (expression in cells treated with control skin-draining lymph-node CM and isotype control = 1). Mean ± s.e.m. ($n = 4$). (**l**) IL-17 concentration in serum. Mean ± s.e.m. ($n = 10$). (**m**) G-CSF concentration in the serum. Mean ± s.e.m. ($n = 6$). (**n**) Representative FACS profiles of CD11b$^+$ Gr-1$^+$ granulocytes ($n = 8$). (**d**, **e**, **j**, **k**) All values are normalized to *GAPDH*. (**d**–**n**) 8–12-week-old mice were used. Statistical significance was assessed using a Student's *t*-test. *$P < 0.05$; **$P < 0.01$. ND, not detected.

increased expression of *IL-23p19*, regardless of their differentiation status (Fig. 5e). Thus, loss of PLCδ1 from keratinocytes did not upregulate *IL-23* in this *in vitro* system, suggesting that interactions between PLCδ1-deficient keratinocytes and other epidermal cells may be required for IL-23 production. We then examined whether the epidermal increase in IL-23 was linked to IL-17 upregulation in the *cKO* epidermis. IL-23 was neutralized using its specific p19 subunit antibody, and *IL-17* expression was then examined in control and *cKO* epidermal sheets. *IL-17* mRNA levels in the *cKO* epidermal sheet were clearly decreased in the presence of anti-IL-23p19 neutralizing antibody, compared with levels in the presence of isotype control (Fig. 5f), indicating that IL-23 has a critical role in *IL-17* upregulation in *cKO* epidermis. We then investigated the mechanisms responsible for IL-23 upregulation by assessing